AGU100 ADVANCING EARTH AND SPACE SCIENCE

Paleoceanography and Paleoclimatology

RESEARCH ARTICLE
10.1029/2018PA003408

Key Points:
- Water sinking south of modern North Atlantic subtropical front partly replaced Antarctic Intermediate Water especially in northern tropics
- Preformed and total phosphate concentrations in glacial Antarctic Intermediate Water and North Atlantic Deep Water were lower than modern
- A partial replacement of AAIW by subtropical waters and low preformed nutrients in glacial AAIW weakened the tropical phosphate maximum

Supporting Information:
- Supporting Information S1
- Data Set S1

Correspondence to:
D. W. Oppo,
doppo@whoi.edu

Citation:
Oppo, D. W., Gebbie, G., Huang, K.-F., Curry, W. B., Marchitto, T. M., & Pietro, K. R. (2018). Data constraints on glacial Atlantic water mass geometry and properties. *Paleoceanography and Paleoclimatology*, *33*, 1013–1034. https://doi.org/10.1029/2018PA003408

Received 21 MAY 2018
Accepted 5 SEP 2018
Accepted article online 11 SEP 2018
Published online 27 SEP 2018

Data Constraints on Glacial Atlantic Water Mass Geometry and Properties

Delia W. Oppo[1], Geoffrey Gebbie[2], Kuo-Fang Huang[1,3], William B. Curry[1,4], Thomas M. Marchitto[5], and Kathryn R. Pietro[1]

[1]Department of Geology and Geophysics, Woods Hole Oceanographic Institution, Woods Hole, MA, USA, [2]Department of Physical Oceanography, Woods Hole Oceanographic Institution, Woods Hole, MA, USA, [3]Academia Sinica, Institute of Earth Sciences, Taipei, Taiwan, [4]Bermuda Institute of Ocean Sciences, St. George's, Bermuda, [5]Department of Geological Sciences and Institute of Arctic and Alpine Research, University of Colorado Boulder, Boulder, CO, USA

Abstract The chemical composition of benthic foraminifera from marine sediment cores provides information on how glacial subsurface water properties differed from modern, but separating the influence of changes in the origin and end-member properties of subsurface water from changes in flows and mixing is challenging. Spatial gaps in coverage of glacial data add to the uncertainty. Here we present new data from cores collected from the Demerara Rise in the western tropical North Atlantic, including cores from the modern tropical phosphate maximum at Antarctic Intermediate Water (AAIW) depths. The results suggest lower phosphate concentration and higher carbonate saturation state within the phosphate maximum than modern despite similar carbon isotope values, consistent with less accumulation of respired nutrients and carbon, and reduced air-sea gas exchange in source waters to the region. An inversion of new and published glacial data confirms these inferences and further suggests that lower preformed nutrients in AAIW, and partial replacement of this still relatively high-nutrient AAIW with nutrient-depleted, carbonate-rich waters sourced from the region of the modern-day northern subtropics, also contributed to the observed changes. The results suggest that glacial preformed and remineralized phosphate were lower throughout the upper Atlantic, but deep phosphate concentration was higher. The inversion, which relies on the fidelity of the paleoceanographic data, suggests that the partial replacement of North Atlantic sourced deep water by Southern Ocean Water was largely responsible for the apparent deep North Atlantic phosphate increase, rather than greater remineralization.

Plain Language Summary The Atlantic circulation system, characterized by northward upper ocean flow and deep southward flow, exerts tremendous influence on the distribution of salt, heat, nutrients, and carbon in the world's oceans, with consequences on surface climate, marine ecosystems, and atmospheric carbon dioxide levels. Reconstructing past ocean circulation and the distribution of ocean properties is challenging, in large part because paleoceanographic proxies may reflect changes in more than one oceanographic variable. We combine new data, published data, and a model to provide new insights into how and why the nutrient distribution of the Atlantic at the peak of the last ice age, approximately 23,000 to 19,000 years ago, was different from modern. The results indicate links between glacial properties of waters sinking in the high-latitude surface ocean, their pathways and subsurface mixtures, and the distribution of nutrients in the glacial ocean.

1. Introduction

Accurate reconstructions of ocean subsurface properties and circulation during the Last Glacial Maximum (LGM; ~23,000–19,000 years before present) are needed to understand the ocean's role in glacial to interglacial climate change, including the lower concentration of CO_2 in the glacial atmosphere. Many early and recent studies focus on the leverage the Southern Ocean has to modify oceanic carbon storage and atmospheric CO_2 by changes in physical stratification and the biologic pump (e.g., Adkins et al., 2002; Ferrari et al., 2014; François et al., 1997; Marzocchi & Jansen, 2017; Sigman et al., 2007, 2010; Sigman & Boyle, 2000; Toggweiler, 1999). Several studies underscore the importance of changes in the fraction of deep water masses with high versus low preformed nutrients for the biologic pump and atmospheric CO_2 (e.g., Ito & Follows, 2005; Kwon et al., 2012; Menviel et al., 2017; Schmittner & Lund, 2015; Sigman & Haug, 2003).

Despite decades of research, glacial water mass boundaries and deepwater properties are still uncertain. Benthic foraminiferal carbon isotope ($\delta^{13}C$), cadmium/calcium (Cd/Ca), and radiocarbon data may imply a shallower but persistent North Atlantic Deep Water (NADW) during the LGM (e.g., Boyle & Keigwin, 1987; Curry & Oppo, 2005; Duplessy et al., 1988; Skinner et al., 2017), and sedimentary 231-Protactinium to 230-Thorium ($^{231}Pa/^{230}Th$) ratios may imply a weaker Atlantic Meridional Overturning Circulation (AMOC) with stronger shallow overturning (Gherardi et al., 2005; Lippold et al., 2016; McManus et al., 2004). However, recent studies challenge the notion that glacial NADW shoaled as much as initially believed and suggest instead that glacial benthic foraminiferal $\delta^{13}C$ and Cd/Ca values also reflect significantly greater storage of respired carbon and nutrients than modern (Freeman et al., 2016; Gebbie, 2014; Howe et al., 2016; Spooner et al., 2018). In addition, the interpretation of sediment $^{231}Pa/^{230}Th$ data is confounded by uncertainties in the analysis of these data (Burke et al., 2011) and by spatial variations in scavenging intensity (Hayes et al., 2015). Seawater properties and the northward extent of Antarctic Intermediate Water (AAIW) in the glacial tropical Atlantic are also not well resolved, although several studies suggest that its preformed properties changed (Makou et al., 2010; Oppo & Horowitz, 2000; Poggemann et al., 2017). In general, recent simulations using coupled models forced by glacial boundary conditions simulate a stronger glacial AMOC, contrasting with the widely held proxy-based view of a more sluggish glacial circulation (Muglia & Schmittner, 2015; Sherriff-Tadano et al., 2017). Furthermore, several glacial simulations do not exhibit the shallower glacial NADW inferred from paleoceanographic data, possibly because glacial Antarctic stratification is too weak in those simulations (Marzocchi & Jansen, 2017). However, because of limitations in the proxies, and the opposing view from glacial simulations, whether the AMOC was shallower or weaker than modern during the LGM is still uncertain.

Proxy data from glacial marine sediments are sometimes used to select among glacial simulations with different water mass distributions and overturning rates (e.g., Butzin et al., 2005; Hesse et al., 2011; Menviel et al., 2017) or to estimate subsurface glacial water masses and properties (Gebbie, 2014; Gebbie et al., 2015; Kurahashi-Nakamura et al., 2017), the strategy we employ here. Although the spatial coverage of glacial benthic $\delta^{13}C$ is better than for other subsurface proxies, there are still regions with little data (Gebbie et al., 2015). Moreover, interpretation of variations in benthic $\delta^{13}C$ is not straightforward, as the $\delta^{13}C$ of dissolved inorganic carbon ($\delta^{13}C_{DIC}$) is influenced by several processes (e.g., Lynch-Stieglitz et al., 1995) and benthic $\delta^{13}C$ values are sometimes offset from $\delta^{13}C_{DIC}$ (Schmittner et al., 2017, and references therein). The spatial distribution of glacial benthic Cd/Ca data, which provides information on phosphate concentration (Boyle, 1988a) and helps isolate the air-sea gas exchange signature of benthic $\delta^{13}C$ ($\delta^{13}C_{AS}$; Lynch-Stieglitz et al., 1996), is even more limited (Marchitto & Broecker, 2006). Quantitative indicators for other ocean properties, such as benthic boron/calcium (B/Ca) estimates for carbonate saturation state (e.g., Yu et al., 2010), are scarce. The shallow tropical Atlantic is poorly represented in the LGM databases of all these proxies, and yet as we discuss below, its properties change significantly on glacial-interglacial time scales, implying variations in water mass sources, their preformed properties, and/or residence times (e.g., Freeman et al., 2015; Poggemann et al., 2017; Weldeab et al., 2016).

Using stable isotopes and elemental ratios of benthic foraminifera, we reconstruct variations in nutrient and carbon cycle parameters in the western tropical North Atlantic, where distribution patterns in the modern ocean are related to water mass mixing and organic matter regeneration as driven by large-scale Atlantic Ocean circulation (section 2.1). We present updated sections of glacial western Atlantic $\delta^{13}C$, seawater cadmium (CdW), and $\delta^{13}C_{AS}$ estimates and the results of a glacial inversion. The results provide insight into how and why glacial Atlantic water mass fractions and preformed and subsurface properties were different from modern and how these differences influenced water properties in the shallow western tropical Atlantic. The sections and glacial inversion also include new Cd/Ca data from a transect of cores from the Blake Outer Ridge in the western Atlantic, where glacial benthic $\delta^{13}C$ data are already available (Keigwin, 2004).

2. Materials and Methods

2.1. Study Areas and Modern Context

Most of our new western Atlantic data come from sediment cores taken from the Demerara Rise, a bathymetric feature in the western tropical North Atlantic, including data from several cores at

Table 1
Core Locations

Core ID	Latitude	Longitude	Core depth (m)
Demerara Rise			
KNR-197-3-23GGC	7.58	−53.92	376
KNR-197-3-47CDH	7.70	−52.79	671
KNR-197-3-46CDH	7.70	−53.79	947
KNR-197-3-9GGC	7.93	−53.79	1,100
KNR-197-3-53GGC	8.20	−53.18	1,272
KNR-197-3-45GGC	8.3	−53.17	1,394
KNR-197-3-36GGC	8.42	−52.86	2,422
KNR-197-3-60GGC	8.44	−52.97	2,642
Blake Outer Ridge			
KNR-140-63JPC	32.99	−76.41	900
KNR-140-51GGC	32.78	−76.12	1,790
KNR-140-51GGC	32.78	−76.12	1,790
KNR-140-50GGC	32.75	−76.24	1,903
KNR-140-64GGC	32.74	−76.13	2,101
KNR-140-64GGC	32.74	−76.13	2,101
KNR-140-67JPC	32.74	−76.13	2,102
KNR-140-43GGC	32.02	−76.07	2,590
KNR-140-37JPC	31.69	−75.43	2,975
KNR-140-39GGC	31.67	−75.42	2,975
KNR-140-26GGC	29.70	−73.40	3,845
KNR-140-28GGC	30.10	−73.84	4,211
KNR-140-12JPC	29.08	−72.90	4,250
KNR-140-22JPC	28.03	−74.41	4,712

underrepresented depths (<1,000 m; Table 1 and Figures S1 and S2 in the supporting information). Fine-grained terrigenous sediment enters the ocean with Amazon River discharge and is transported northward in the North Brazil Current (Mario & Michel, 1998), resulting in expanded sedimentary sections shallow on the rise.

Relatively low salinity between ~400 and 1,000-m water depth in our Demerara Rise study area reflects the influence of Subantarctic Mode Water, AAIW, and Upper Circumpolar Deep Water, which have been diluted by mixing with saltier South Atlantic Central Waters and Mediterranean Outflow Waters, above and below, respectively (Figure S3 in the supporting information). In keeping with previous studies, and for simplicity, we refer to the combined shallow southern water masses as AAIW. In the modern ocean, northward flowing AAIW contributes substantially to the return flow that compensates for southward NADW export at depth (Schmitz & McCartney, 1993). AAIW is also a significant source of nutrients to the Atlantic basin (Sarmiento et al., 2004; Tuerena et al., 2015).

$\delta^{13}C_{DIC}$ and Cd concentration are negatively (Kroopnick, 1985) and positively (Boyle, 1988a) correlated to phosphate concentration, respectively, although $\delta^{13}C_{DIC}$ is also influenced by the air-sea gas exchange that occurs before surface source waters are transported to depth (e.g., Lynch-Stieglitz et al., 1995). Compared to NADW, AAIW has lower $\delta^{13}C_{DIC}$ (Kroopnick, 1985) and higher phosphate (Bainbridge, 1981) and cadmium (Marchitto & Broecker, 2006; Middag et al., 2018; Xie et al., 2015; Figures S4–S6 in the supporting information). This is because North Atlantic waters are supplied from the nutrient-depleted surface and thermocline, whereas AAIW is in part supplied by deeper, nutrient-rich Circumpolar Deep Waters (e.g., Sarmiento et al., 2004). In the western tropical Atlantic, the local minimum in $\delta^{13}C_{DIC}$ and maximum in phosphate (and cadmium) above ~1,100 m are due to the regeneration of organic matter and accumulation of respired carbon and phosphate, respectively.

The contributions of remineralized components, $\delta^{13}C_{DIC}^{remin}$ and PO_4^{remin}, were estimated from a global hydrographic inversion (Gebbie, 2014) of modern-day seawater data of $\delta^{13}C_{DIC}$ (Schmittner et al., 2013), $\delta^{18}O$ (Schmidt, 1999), temperature, salinity, phosphate, nitrate, and dissolved oxygen (Gouretski & Koltermann, 2004). The inversion assumes a fixed stoichiometric ratio between remineralized phosphate and $\delta^{13}C_{DIC}$ (1 μmol/kg: −1.1‰; all $\delta^{13}C$ values discussed are relative to Vienna Pee Dee Belemnite standard) in accordance with the global mean DIC and photosynthesis (Broecker & Maier-Reimer, 1992), although this is clearly a simplification. The resulting three-dimensional $\delta^{13}C_{DIC}^{remin}$- and PO_4^{remin}-gridded products are mapped onto the western Atlantic GEOSECS track (e.g., Kroopnick, 1985) using two-dimensional (2-D) linear interpolation in the horizontal (Figures S7 and S8 in the supporting information). The intermediate-depth minimum and maximum, respectively, conform to remineralized phosphate patterns documented previously (Gruber & Sarmiento, 2002). The inversion suggests that intermediate-depth tropical Atlantic $\delta^{13}C_{DIC}$ is reduced by as much as 1‰ by remineralization, and phosphate increased by as much as 0.9 μmol/kg. Of the 1‰ $\delta^{13}C_{DIC}$ decrease (0.9-μmol/kg phosphate increase), about 60% occurs near the formation sites of AAIW, and the rest occurs along the subtropical and tropical journey of the water. Preformed $\delta^{13}C_{DIC}$ and phosphate (e.g., Figure S9 in the supporting information) are calculated by subtracting the remineralized estimates from total phosphate. The ratio of remineralized to total phosphate, which is a measure of the efficiency of the soft tissue pump (Ito & Follows, 2005), ranges between ~0.1 and 0.4, with lowest values in the shallow subtropics and highest in the shallow tropics (Figure S10 in the supporting information). Our estimates of remineralized phosphate, and the phosphate to total phosphate ratio, are lower than estimated previously using apparent oxygen utilization, as that method overestimates remineralized phosphate in cold undersaturated waters (Ito & Follows, 2005). Conversely, our preformed phosphate estimates are higher.

$\delta^{13}C_{AS}$ isolates the abiotic component of $\delta^{13}C_{DIC}$ by normalizing to zero phosphate. In the modern ocean, the $\delta^{13}C_{AS}$ of Southern Ocean water masses, especially AAIW, is high, whereas that of NADW is low (Figure S11 in the supporting information; Lynch-Stieglitz et al., 1994, 1995). The high $\delta^{13}C_{AS}$ of AAIW

reflects its relatively high preformed $\delta^{13}C_{DIC}$ for its preformed phosphate value (e.g., Oppo & Fairbanks, 1987). Because it is nearly conservative, $\delta^{13}C_{AS}$ may help identify the contribution of northern versus southern sources to the ocean interior (Lynch-Stieglitz et al., 1994, 1995).

Remineralization also causes local minima in the carbonate ion concentration ($[CO_3^{=}]$) and the difference between $[CO_3^{=}]$ and its saturation value with respect to calcite, that is, the carbonate saturation state ($\Delta [CO_3^{=}]$). Carbonate ion concentrations and carbonate saturation states (with respect to calcite) in the modern ocean were calculated using CO2SYS diagnostic routines with default settings (Lewis & Wallace, 1998) and gridded fields of dissolved inorganic carbon and total alkalinity from GLODAP version 1 (Key et al., 2004), and World Ocean Circulatoin Experiment (WOCE) temperature, salinity, and phosphate values (Gouretski & Koltermann, 2004) mapped onto the GLobal Ocean Data Analysis Project (GLODAP) gridded locations as inputs. The $[CO_3^{=}]$ section shows a vertical structure consistent with the Atlantic water masses: low ($<$90 μmol/kg) $[CO_3^{=}]$ in AAIW and Antarctic Bottom Water, with higher ($>$90-μmol/kg) concentrations in NADW (Figure S12 in the supporting information). Benthic foraminiferal B/Ca records, however, may be more sensitive to $\Delta [CO_3^{=}]$ (Yu et al., 2008). While the overall $\Delta [CO_3^{=}]$ pattern is a decrease with depth due to the effect of pressure on the saturation value, tropical intermediate waters are still distinguished by a local minimum with values less than 30 μmol/kg (Figure S13 in the supporting information).

We also present unpublished benthic Cd/Ca data from the Blake Outer Ridge (Figure S2 in the supporting information). Core sites shallower than 4,000 m are largely within modern NADW, and deeper sites are increasingly influenced by Southern Ocean Water (SOW; Keigwin, 2004). Glacial benthic $\delta^{13}C$ data from these sites suggest that the core of high-$\delta^{13}C$ glacial NADW was above 2,000 m with an increase in the fraction of low-$\delta^{13}C$ SOW below 2,000 m (Keigwin, 2004), in agreement with early reconstructions of glacial North Atlantic water mass geometry (e.g., Boyle & Keigwin, 1987; Duplessy et al., 1988), and informing later ones (e.g., Curry & Oppo, 2005).

2.2. Core Top Measurements

We measured $\delta^{18}O$ and $\delta^{13}C$ on the calcitic benthic foraminifer *Cibicidoides pachyderma* or *C. wuellerstorfi* in the top samples of Demerara Rise multicores ranging in water depth from 383 to 3,328 m. The $\delta^{13}C$ values of most *Cibicidoides* species are generally believed to record the $\delta^{13}C_{DIC}$ (Belanger et al., 1981; Curry et al., 1988; Duplessy et al., 1984), although there is some evidence that *C. pachyderma* inhabits a shallow infaunal habitat (typically in the top centimeter; Fontanier et al., 2006); it has also been found deeper, within burrows (McCorkle et al., 1997). Foraminiferal $\delta^{18}O$ variations reflect some combination of variations in temperature of calcification (Emiliani, 1955) and $\delta^{18}O$ of seawater (e.g., Lynch-Stieglitz et al., 1999; Shackleton, 1967).

We made measurements of Cd/Ca in three species of benthic foraminifera from these same multicore tops: the epifaunal species *C. wuellerstorfi*, the infaunal species *Uvigerina perigrina*, and *C. pachyderma*. Cadmium concentration was determined on water samples collected on hydrocasts at the Demerara Rise. Comparison of seawater cadmium and core top benthic foraminiferal Cd/Ca data resulted in a slight revision of distribution coefficients (section 3.1). We also present multicore top boron/calcium (B/Ca) data for *C. pachyderma* and *U. peregrina*. B/Ca values of some *Cibicidoides* species are correlated to carbonate saturation state ($\Delta[CO_3^{2-}]$; Yu & Elderfield, 2007).

2.3. Downcore Measurements

We sampled eight cores from the Demerara Rise (376–2,642-m water depth) at 2 to 8-cm intervals. We measured $\delta^{18}O$ and $\delta^{13}C$ on several individual tests, if possible, of the benthic foraminifera *C. pachyderma* (shallower cores) and *C. wuellerstorfi* (deeper cores). Neodymium isotope data and radiocarbon chronologies for KNR197-3-46CDH and KNR197-3-9GGC were presented earlier (Huang et al., 2014), and radiocarbon chronologies have been updated with the Marine13 calibration (Reimer et al., 2013; supporting information tables). The bottom of a third core studied previously, KNR197-3-25GGC, is dated to approximately 19,500 years ago (Huang et al., 2014). To acquire full glacial values from this water depth (~670 m), we worked on companion piston core KNR197-3-47CDH and dated its glacial section. Radiocarbon dates also constrain the glacial sections of the other Demerara Rise cores used in this study (supporting information tables).

We measured elemental ratios of benthic foraminifera (*C. pachyderma*, *C. wuellerstorfi*, and *U. peregrina*) from glacial sections of six of these Demerara Rise cores and of benthic foraminifera (*Hoeglundina elegans*,

C. wuellerstorfi, *U. peregrina*, or *Nuttaloides umbonifera*) from a depth transect of 12 cores (900–4,700 m) from the Blake Outer Ridge in the western Atlantic (~28–33°N; Table 1). Glacial levels for the Blake Outer Ridge cores were established previously from radiocarbon dates and oxygen isotope data (Curry & Oppo, 2005; Keigwin, 2004). Cd/Ca values were converted to glacial cadmium water estimates (CdW) using the revised distribution coefficients (section 3.1). CdW was converted to phosphate using the nonlinear relationship in Elderfield and Rickaby (2000). Following Lynch-Stieglitz et al. (1996), the glacial equation for estimating $\delta^{13}C_{AS}$ assumes a 4% increase in the mean ocean dissolved inorganic carbon inventory, an associated mean ocean $\delta^{13}C$ decrease of 0.3‰, and a 2% increase in the $\delta^{13}C$ of organic matter. The resulting equations used are

$$\delta^{13}C_{AS} = \delta^{13}C_{DIC} + 1.1^{*}PO_4^{2-} - 2.75 \text{ (modern) and}$$
$$\delta^{13}C_{AS} = \delta^{13}C_{DIC} + 0.95^{*}PO_4^{2-} - 2.15 \text{ (glacial)}.$$

Stable isotope measurements were made at the Woods Hole Oceanographic Institution (WHOI) on a Finnigan MAT253 mass spectrometer equipped with an integrated automated carbonate device using standard procedures (Ostermann & Curry, 2000). Data were converted to Vienna Pee Dee Belemnite using NBS-19 standards analyzed in each run. Measurement precision, as determined by NBS-19, was ±0.05‰ for $\delta^{13}C$ and ±0.08‰ for $\delta^{18}O$.

Elemental ratios (Cd/Ca, B/Ca, among others) were measured on 5–15 pooled tests of the benthic foraminifera. Foraminifera were cleaned following the full trace metal protocol (Boyle & Keigwin, 1985; Rosenthal et al., 1995). Demerara Rise core top and glacial measurements on *C. pachyderma* from core 46CDH were collected at WHOI, and new glacial measurements of Blake Outer Ridge cores were determined at the University of Colorado, respectively, both on a Thermo-Finnigan Element2 sector field single collector inductively coupled plasma mass spectrometer (ICP-MS) following the method of Rosenthal et al. (1999) and subsequent modifications (Huang et al., 2008; Lear et al., 2002; Marchitto, 2006). Glacial measurements on *U. peregrina* from core 46CDH and on the glacial sections of other Demerara Rise cores were generated at Academia Sinica on a Thermo-Scientific Element XR sector field single-collector ICP-MS, using the same methods. At the time of these measurements, the long-term precision (±2 relative standard deviations; RSD) for all elemental ratios was better than 3% (2.4% for Cd/Ca and 3% for B/Ca) at WHOI, better than 2.5% at Academia Sinica, and ~3.6% for Cd/Ca at University of Colorado, based on matrix-matched consistency standards.

Cd/Ca of seawater collected on Demerara Rise hydrocasts was also measured at WHOI. Briefly, filtered seawater samples were acidified at sea with ultrapure 11N HCl (BASELINE®, SEASTAR) to pH < 2 and were subsampled (20 ml) into acid-clean 30-ml polypropylene bottles (Nalgene®) in a clean room environment. The 20-ml aliquots were adjusted to pH = 6.0 ± 0.2 by adding ultrapure 11-M ammonia solution (BASELINE®, SEASTAR) for the Cd purification using Chelex-100 resin (Bio-Rad, 200–400 mesh, bed volume: 0.25 ml). After cleaning once with 5-ml 2N HNO_3 and 15-ml deionized water (DIW), the columns were conditioned with 5-ml 1-M ammonium acetate ($NH_4CH_3CO_2$). After sample loading, 14-ml 1-M $NH_4CH_3CO_2$, followed by 0.5-ml DIW, were added to remove matrix elements. Cd was then collected by adding 2-ml DIW and 3-ml 2N HNO_3. The chemical yield for Cd was better than 97 ± 2% (2RSD, $n = 12$) through processing the synthetic seawater standard (doped with 0.020 μg/L of Cd). A series of reference seawater standards were measured to further validate our methodology. The measured Cd concentrations of NASS-5 (0.196 ± 0.004 nM, 2SD, $n = 6$), CASS-5 5 (0.240 ± 0.005 nM, 2SD, $n = 6$), and SAFe-D2 (6.99 ± 0.35 nM, 2SD, $n = 6$) are in excellent agreement with the published results (Milne et al., 2010, and references therein). Ca concentrations were calculated based on the salinity data obtained from the CTD (conductivity, temperature, depth instrument package).

2.4. Data Sources for Glacial Western Atlantic Sections and the Glacial Solution

The western Atlantic glacial $\delta^{13}C$ section includes published benthic data compiled previously (Curry & Oppo, 2005), data published since then (Burckel et al., 2015; Freeman et al., 2015; Hodell et al., 2008, 2010; Hoffman & Lund, 2012; Keigwin & Swift, 2017; Lund et al., 2015; Lynch-Stieglitz et al., 2014; Oppo et al., 2015; Poggemann et al., 2017; Praetorius et al., 2008; Rickaby & Elderfield, 2005; Tessin & Lund, 2013; Thornalley et al., 2010; Voigt et al., 2017), and our new data from the eight cores on the Demerara Rise, ranging in water depth from 376 to 2,642 m (Table 1 and supporting information tables). The Western Atlantic CdW section includes data compiled previously (Marchitto & Broecker, 2006), data published since then (Makou et al.,

Table 2
Glacial Planktonic Isotope Data Used in Inversion

Core ID	Latitude	Longitude	Species	LGM-Holocene $\delta^{13}C$	LGM-Holocene $\delta^{18}O$	Reference
KNR197-3-46CDH	7.7	−53.8	*G. ruber*	0.53	−1.81	This paper
OCE205-103GGC	26	−78.1	*G. sacculifer*	−0.09	−2.03	This paper
EW9209-1JPC	5.9	−44.2	*G. sacculifer*	0.37	−1.64	Curry and Oppo (1997)
KNR195-5-36GGC	−27.3	−46.5	*G. ruber*	0.14	−1.39	This paper
MD02-2594	−34.7	17.3	*G. ruber*	0.35	−1.24	Dyez et al. (2014)

2010; Poggemann et al., 2017), and new data from the Demerara Rise and Blake Outer Ridge. Revised distribution coefficients, discussed below, were applied to all published and new Cd/Ca data (supporting information tables).

The inversion is also informed by Cd/Ca and $\delta^{13}C$ data from the eastern basin compiled by Marchitto and Broecker (2006; Figure S14 in the supporting information). An earlier inversion of glacial data gave unrealistically low $\delta^{13}CAS$ values in the surface South Atlantic (not shown). To address this issue, we included planktonic $\delta^{13}C$ data from two South Atlantic cores, one each from the eastern and western South Atlantic (Dyez et al., 2014; unpublished data, supporting information tables). We also included planktonic $\delta^{13}C$ data from a published record (Curry & Oppo, 1997) and two unpublished records (supporting information tables and Table 2) to help constrain from the tropical and subtropical North Atlantic glacial surface $\delta^{13}C$ values. Because $\delta^{13}C$ values of planktonic foraminifera are offset from seawater and are often a function of size (e.g., Oppo & Fairbanks, 1989; Spero & Williams, 1988), glacial-Holocene planktonic $\delta^{13}C$ differences were subtracted from modern values to assign glacial values at each site.

2.5. Glacial Inversions

Here we seek three-dimensional (3-D) property distributions that fit the benthic observations within uncertainty and also satisfy a unique (given our assumptions) water mass decomposition for each location on a global grid with 4° × 4° horizontal resolution and 33 vertical levels with enhanced resolution near the surface. The water mass fractions in each cell of the 3-D grid are estimated by taking into account the geometric constraints inherent in an equilibrium circulation, where the path of a water mass must be continuous from source to destination, as described by Gebbie (2014). A least squares method is used to solve for a water mass distribution that fits 127 $\delta^{18}O$, 156 $\delta^{13}C$, and 115 CdW glacial observations from the Atlantic Ocean (section 2.4 and Figure S14 in the supporting information), as well as glacial sea surface temperature estimates (Kucera et al., 2006; MARGO Project Members, 2009). As in Gebbie (2014), $\delta^{18}O$ of calcite ($\delta^{18}Oc$) is assumed to follow the relationship provided in equation (1) of Bemis et al. (1998) and a 0.27‰ offset in $\delta^{18}O$ scales. Uncertainties assumed on glacial values are as in Gebbie (2014). The glacial inversion is not analyzed in the Indo-Pacific because of the lack of constraints there.

Relevant details of the water mass decomposition technique are emphasized next, but the reader is referred to previous publications for more details (Gebbie, 2014; Gebbie et al., 2015, 2016). The output of the inversion includes more than the water mass geometry, as this knowledge is also used to reconstruct 3-D global distributions of multiple properties simultaneously. The conservative tracers, temperature, preformed salinity, and $\delta^{18}O$ of seawater, are directly computed from water mass fractions, but the nonconservative tracers (here $\delta^{13}C_{DIC}$, PO_4^{3-}, NO_3^-, and O_2) also require information about remineralization at each subsurface grid cell. Thus, each nonconservative property in a given cell is due to the contribution from multiple water masses and an additional source. The local source of remineralized phosphate, q^{remin} (and of other remineralized material related by stoichiometric ratios), is given by the product of remineralization rates and residence time in a given grid cell. In order to keep the vertical structure of remineralization realistic, it is assumed to have a spatial pattern nearly identical to (within 0.001% of) the modern-day reference solution (Gebbie, 2014). This source is a maximum in the intermediate-depth ocean, where the seawater residence time is increased relative to the upper ocean, but the vertical fluxes of particulate organic matter are still significant. The accumulation of remineralized phosphate, PO_4^{remin}, is defined to be the difference between the actual phosphate concentration and preformed phosphate (i.e., the concentration of a hypothetical conservative tracer with

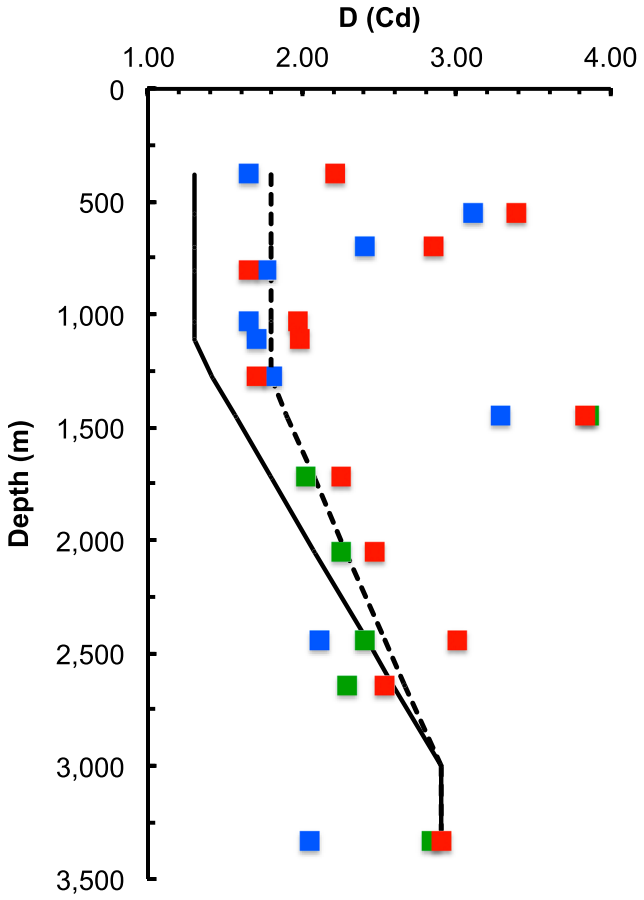

Figure 1. Estimated cadmium distribution coefficients in core top foraminifera from the Demerara Rise: *U. peregrina* (red), *C. pachyderma* (blue), and *C. wuellerstorfi* (green). Dashed line marks our best estimate of the depth-dependent distribution for calcitic foraminifera. Estimate from Boyle (1992) is shown as a solid line.

phosphate surface values; Gruber & Sarmiento, 2002). Thus, PO_4^{remin} depends on both the local source, q^{remin}, and the transport of phosphate by the circulation. Given that the local source is held nearly constant, any changes in PO_4^{remin} must be due to the transport of phosphate by the circulation.

A limitation of the inversion is that water mass fractions are explicitly solved but rates of circulation are not. Both q^{remin} and PO_4^{remin} contain information about the relative rates of biological and physical processes, but we cannot unambiguously determine how much each process contributes to differences between the glacial solution and modern.

Recognizing that the paleo-observations are uncertain and have spatial gaps, we augment our solution method by enforcing gravitational stability and the nonnegativity of tracer concentrations. For grid cells without data, the reconstruction is informed by the upstream and downstream glacial data and modern circulation and length scales. Thus, although the solution fits the data, it may be biased by the prior assumption of a modern-like circulation. It is also worth noting that we do not provide subsurface temperature or salinity information, and thus, neither of these fields is independently well constrained by the inversion. Benthic $\delta^{18}O$ observations permit the inversion to reconstruct plausible density fields, however, with greater stratification in the glacial inversion than in the modern (not shown).

Here we refer to waters that sink north of the modern-day boundary between the North Atlantic subtropical and subpolar gyres (including Nordic Overflows and Labrador Sea waters) collectively as *NADW* and waters that sink south of the modern-day South Atlantic subtropical/subpolar gyre boundary as *AAIW* or *SOW* depending on depth and context. Waters having a surface source equatorward of the modern-day gyre boundaries are referred to as *subtropical* waters. Like a previous inversion that reconstructed glacial water mass fractions (Gebbie, 2014), we use $\delta^{18}O$, $\delta^{13}C$, and CdW estimates from the Atlantic only, as detailed in section 2.4.

3. Core Top and Downcore Data

3.1. Cd Distribution Coefficient

We measured Cd/Ca on calcitic foraminifera (*C. pachyderma*, *C. wuellerstorfi*, and *U. peregrina*) from the top centimeter of 10 multicores from the Demerara Rise, ranging in water depth between 383 and 3,328 m, and compared them to the Cd concentration of water collected from hydrocasts to estimate the Cd distribution coefficient (supporting information tables and Figure 1). Benthic Cd/Ca from three multicore tops are higher than expected. Only one of the three samples, from 703-m water depth, had consistently elevated Al/Ca, Fe/Ca, and Mn/Ca, suggesting possible incomplete removal of clays and/or Mn-$CaCO_3$ overgrowths (e.g., Boyle, 1981, 1983), and other samples with similarly elevated values did not have high Cd/Ca values (supporting information tables). Other elemental ratios measured on these samples, including B/Ca in *C. pachyderma* and *U. peregrina*, discussed in the next section, are not anomalous for their depth (supporting information tables), so the reason for the high Cd/Ca values is unclear. Ignoring Cd/Ca data from these three samples, our best estimate of the depth-dependent distribution coefficient for calcitic foraminifera (*C. pachyderma*, *C. wuellerstorfi*, and *U. peregrina*) is $D = 1.8$ for water depth of 1,300 m and shallower, indistinguishable from $D = 1.74$ estimated by Bryan and Marchitto (2010) using core tops from the Florida Straits, but higher than $D = 1.3$ proposed for calcitic species by Boyle (1992). A linear increase of D from 1.8 at 1,300 m to 2.9 at 3,000 m and deeper as suggested by Boyle (1992) accommodates our data reasonably well, and given that we have data from only one core top below ~2,700 m, we adopt the distribution coefficient implied by this

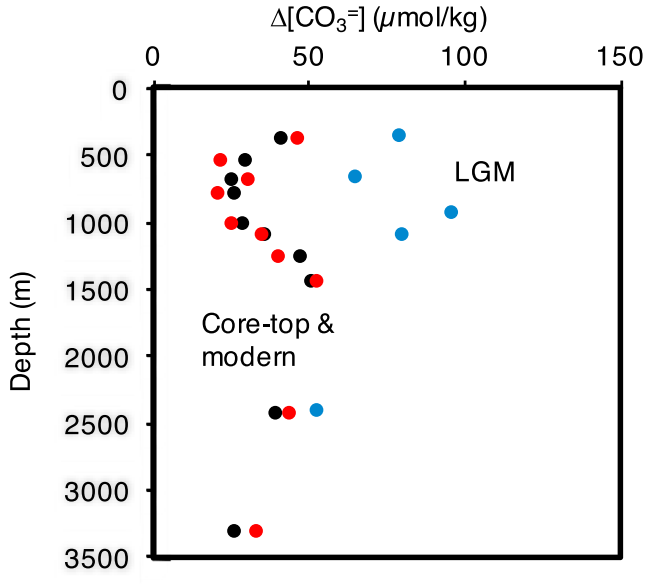

Figure 2. Modern Δ [$CO_3^{=}$] (black) estimated using data from nearby WOCE Line A20 station 74 (8.79°N; 52.66°W, 4631 m; Key et al., 2004) and CO2SYS software (Lewis & Wallace, 1998; Pelletier et al., 2005). Core top (red) and glacial (blue) Δ [$CO_3^{=}$]. All core top data and the four shallowest glacial points are from *C. pachyderma*. The deepest glacial point is from *C. wuellerstorfi*.

trend (Figure 1). We did not measure the aragonitic foraminifera *H. elegans* in our core tops, but given our consistent results for calcitic foraminifera, we adopt Bryan and Marchitto's (2010) value of 1.2 for glacial samples. Considering our typical measurement error of 2.4% on benthic Cd/Ca, and an estimated error on the distribution coefficient of ±0.1, we estimate an average error (2 SE) on CdW estimates of 0.06 nmol/kg. However, as we discuss in greater detail below, contrary to previous results (Boyle, 1988a, 1992; Bryan & Marchitto, 2010), there is a systematic difference among calcitic species in our study area, with *U. peregrina* having higher values in both core-top (Figure 1) and glacial samples, suggesting larger uncertainty than the 2 SE estimate.

3.2. B/Ca Core Top Data

The relationship between B/Ca measured on *C. pachyderma* multicore tops from the Demerara Rise and Δ [$CO_3^{=}$] overlies the published data for *C. mundulus* (Rae et al., 2011; Yu & Elderfield, 2007), although the slope of a calibration using *C. pachyderma* data is steeper (Figure S15 in the supporting information). Using the local, species-specific calibration or the combined data sets, the standard error of prediction (Brownlee, 1965) of Δ [$CO_3^{=}$] is ~10 μmol/kg. We apply the local calibration, and as expected, the core top data capture the water column values and Δ [$CO_3^{=}$] structure (Figure 2). The calibration on the combined *C. mundulus* and *C. pachyderma* data returns a profile with the same shape but a larger range of estimates, exaggerating differences versus depth. We thus apply the local, species-specific calibration to LGM benthic B/Ca data. For *C. wuellerstorfi*, the relationship between bottom water Δ [$CO_3^{=}$] and B/Ca overlies published data (not shown), and we apply the global calibration (Yu & Elderfield, 2007) for glacial data. In agreement with previous studies, *U. peregrina* B/Ca values are low and not very sensitive to bottom water Δ [$CO_3^{=}$] variability (Doss et al., 2018; Yu & Elderfield, 2007), although they do exhibit lower values in the shallow Δ [$CO_3^{=}$] minimum than above or below it (Figure S16 in the supporting information).

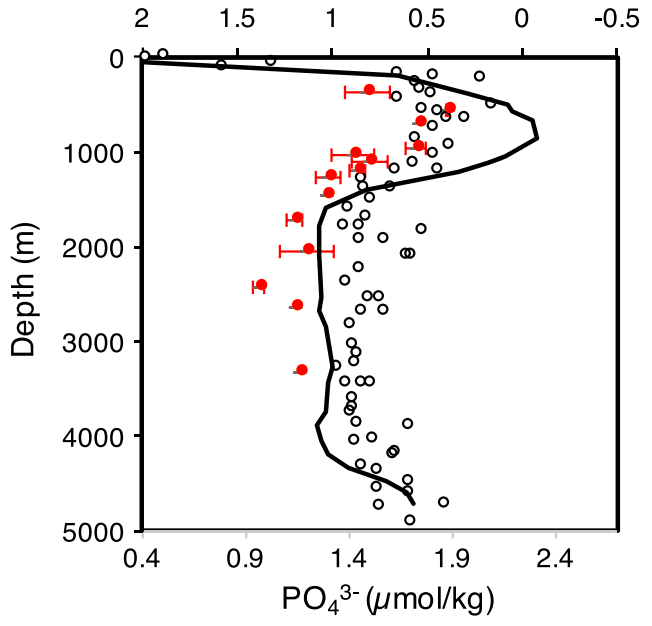

Figure 3. Phosphate (black line, bottom axis; Bainbridge, 1981) and $\delta^{13}C$ (black circles, top axis, reversed; Kroopnick, 1985) from the closest GEOSECS stations (station 37, 12°N, 51°W; stations 39, 4°N, 39°W). Multicore top benthic $\delta^{13}C$ (red) shown with one standard error.

3.3. Core Top $\delta^{13}C$ Data

$\delta^{13}C$ measurements from multicore tops from 383 to 1,452 m water depths are on *C. pachyderma*, and measurements on deeper cores (1,720 to 3,328 m) are on *C. wuellerstorfi*, reflecting their relative abundances in the core top sediment. The core top $\delta^{13}C$ profile exhibits the expected vertical structure, with lowest values within the $\delta^{13}C$ minimum/phosphate maximum and higher values above and below (Figure 3). Within the $\delta^{13}C_{DIC}$ minimum/phosphate maximum, benthic (*C. pachyderma*) $\delta^{13}C$ values are within error of values measured at the closest GEOSECS stations (Kroopnick, 1985) but benthic values from the shallowest site and deeper sites (mostly *C. wuellerstorfi* for the latter) are typically higher than $\delta^{13}C_{DIC}$ by ~0.3‰. A number of factors might have contributed to this offset. First, it is possible that the reported $\delta^{13}C_{DIC}$ values are erroneously lower than $\delta^{13}C_{DIC}$. However, while not as complete as the GEOSECS vertical $\delta^{13}C$ profile, more recent measurements from a nearby station (Key et al., 2004) are consistent with the GEOSECS values. The shallowest core and those from ~1,300 m and deeper have short Holocene sections (~10–60 cm compared to >100 cm from cores from 650 to 950 m; Figure S17 in the supporting information and supporting information), indicating lower Holocene accumulation rates, and the *Cibicidoides* from below the core tops often have higher $\delta^{13}C$ values than those from within the core tops. Thus, we might have systematically picked foraminifera that were older than the youngest sediment deposited (top centimeter). We

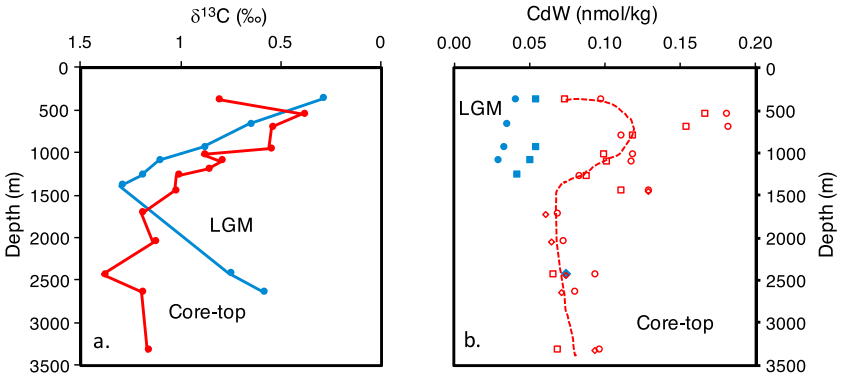

Figure 4. Glacial versus core top (a) $\delta^{13}C$ (reversed axis) and (b) CdW. Red and blue symbols denote core top and glacial estimates, respectively. Diamonds, squares, and circles in (b) denote *C. wuellerstorfi* (including one glacial point at ~3,500 m that has the same value as a core top point), *C. pachyderma*, and *Uvigerina*, respectively. Red dashed line in (b) drawn to highlight the modern maximum centered at ~750-m water depth.

consider such a systematic bias unlikely and moreover, one foraminifer that contained protoplasm as indicated by Rose Bengal stain (Murray & Bowser, 2000), suggesting it was not several hundreds to thousands of years old, had values as high as others from the same sample (KNR197–3-63MC; Supplementary Data Tables). A recent evaluation of a global core top database suggests that carbonate saturation and to a smaller extent depth (pressure) may influence benthic $\delta^{13}C$ values, but the data show considerable scatter and the magnitude of the correction, if any, is small and uncertain (Schmittner et al., 2017). Finally, waters from our deeper core sites are unlikely to have experienced a significant decrease in $\delta^{13}C_{DIC}$ due to oceanic uptake of fossil fuel carbon (Schmittner et al., 2017). Thus, we have no satisfactory explanation for the apparently high *C. wuellerstorfi* $\delta^{13}C$ values.

3.4. Downcore Isotope Records

Benthic isotope data and radiocarbon data suggest that sediment disturbances occur in the deglacial section at many of the core sites (Figure S17 in the supporting information). For example, in core 53GGC, two brief excursions to lower $\delta^{18}O$ and lower $\delta^{13}C$ values, centered near ~82.5 and 94.5 cm, have younger radiocarbon dates than sediment above those depths (supporting information tables). Similarly, the excursion to lower $\delta^{18}O$ at 40.5 cm in 36GGC is associated with relatively young radiocarbon ages. Slope instability has been documented to the east of our core transect (Loncke et al., 2009), and our results are consistent with slope instabilities at our deeper core sites as well. Alternatively, the age reversals may be the results of deep burrowing. Regardless of mechanism, radiocarbon dates converted to calendar age (Reimer et al., 2013) using the mean ocean reservoir age (*R*) confirm the glacial levels identified from benthic $\delta^{18}O$ in all cores. Data from these depths were included in our updated glacial $\delta^{13}C$ section, and for a subset of the cores, for the CdW section. Deglacial records from 9GGC and 46CDH will be discussed elsewhere; here we focus on the LGM.

4. Demerara Rise Profiles and Updated Western Atlantic Sections

In this section, we discuss Demerara Rise glacial data and differences from core top data. We present new compilations of western Atlantic glacial $\delta^{13}C$, CdW, and $\delta^{13}C_{AS}$ and superimpose the data on results of the inversion of glacial data. We only discuss features that are directly supported by the western Atlantic data. The glacial solution, which assigns values even where data are lacking, will be discussed in section 5.

4.1. Glacial $\delta^{13}C$

The Demerara Rise glacial $\delta^{13}C$ vertical profile shows a maximum at ~1,400 m with lower values above and below that depth (Figure 4a). Between ~600 and 1,400 m, glacial values are higher than core top values at all depths where there are paired data; the opposite is true at the shallowest core and below 1,400 m. The new glacial western Atlantic section places these features in the broader context of existing data (Figure 5a) and confirms previous observations, with highest $\delta^{13}C$ values in the shallow North Atlantic, a steep vertical gradient in the North Atlantic, lowest values in the deep Atlantic, and low $\delta^{13}C$ values at the

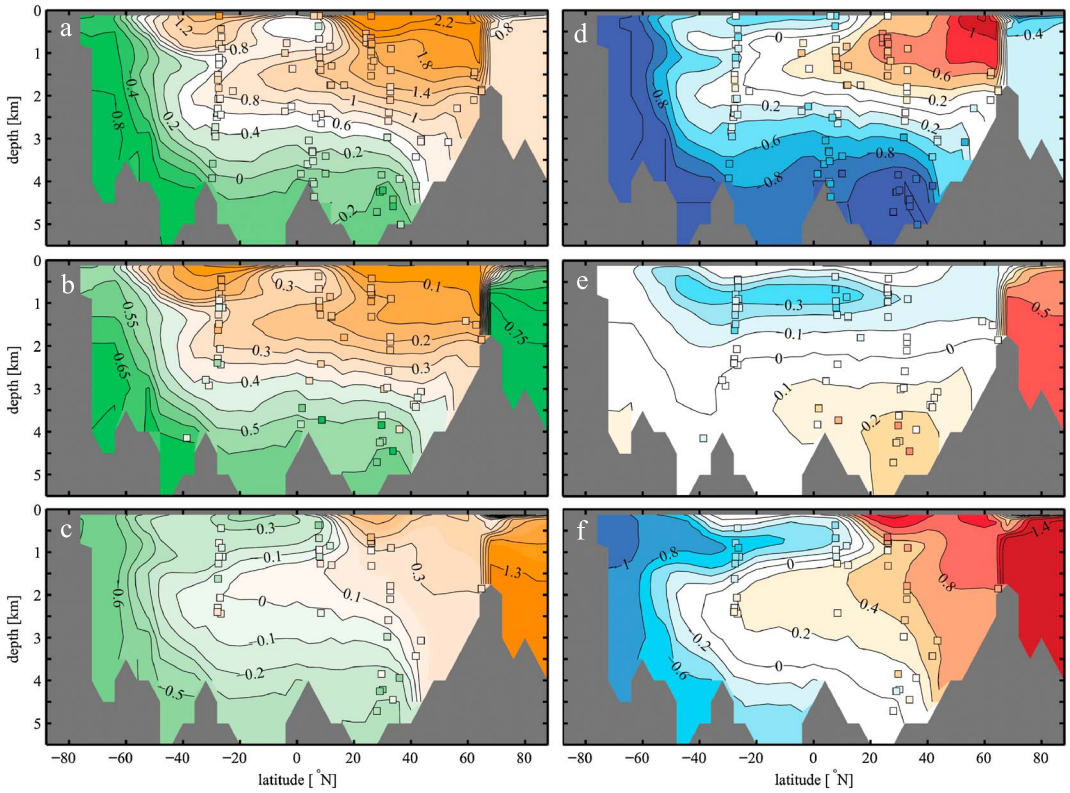

Figure 5. Glacial Western Atlantic (a) $\delta^{13}C$, (b) CdW, and (c) $\delta^{13}C_{AS}$ estimates based on measurements on benthic foraminifera (colored symbols) superimposed on results of the glacial solution along the western Atlantic GEOSECS transect. Glacial-modern differences in (d) $\delta^{13}C$ and (e) CdW and (f) $\delta^{13}C_{AS}$.

approximate depth of modern AAIW in the South Atlantic (e.g., Curry & Oppo, 2005; Duplessy et al., 1988). However, data from Demerara Rise, some used previously (Gebbie et al., 2015), reveal the presence of low-$\delta^{13}C_{DIC}$ waters in the glacial northern tropics, at depths within the modern $\delta^{13}C_{DIC}$ minimum. The data suggest that the largest $\delta^{13}C_{DIC}$ increase and decrease, relative to modern, occurred in the shallow and deep North Atlantic, respectively (Figure 5d). $\delta^{13}C_{DIC}$ also decreased in the shallowest tropical Atlantic and in the upper and deep South Atlantic.

4.2. Glacial CdW

The new Demerara Rise glacial Cd/Ca data from cores between ~380 and 1,270 m suggest lower glacial than Holocene CdW values (Figure 4b). *C. pachyderma* exhibit consistently lower glacial CdW values than *U. peregrina* in cores where both were measured. Notably, however, both species exhibit considerably lower glacial CdW values than the core tops and suggest a significant decrease in phosphate concentrations in the region of the modern phosphate maximum, with glacial waters at the shallow Demerara Rise core sites nearly as nutrient depleted as modern NADW. One data point for *C. wuellerstorfi*, available for the core from ~2,400 m, has a glacial CdW estimate nearly identical to its Holocene value.

For our updated CdW section, we opted to use the *U. peregrina* rather than *C. pachyderma* data for Demerara Rise sites where data for both species were generated (Figure 5b), as the differences of CdW from modern are smaller. For the other Demerara Rise sites, we use *C. pachyderma* (~670 m) and *C. wuellerstorfi* (~2,400 m) data. We do not distinguish among species for published data; some data were generated on mixed calcitic benthics, or on *C. wuellerstorfi*, *H. elegans*, or *Uvigerina* species, but there are not enough data from individual species to make meaningful glacial sections.

Despite the generally low CdW values in the Demerara Rise, the CdW section, which also includes new data from the Blake Outer Ridge, suggests an overall pattern very similar to $\delta^{13}C_{DIC}$ (Figure 5b). However, contrasting with the LGM-modern $\delta^{13}C$ difference, the LGM-modern CdW difference shows only a modest change in

the shallow North Atlantic (Figure 5e). In the deep North Atlantic, glacial CdW is higher than modern, consistent with the lower glacial $\delta^{13}C$ observed there. The largest CdW decrease observed in the western Atlantic data occurs in the shallow tropics. Using *C. pachyderma* instead of *U. peregrina* would not have significantly influenced these results, except that differences from modern are larger. A note of caution on deep North Atlantic CdW estimates is in order: the CdW increase with core depth at the Blake Outer Ridge is mirrored by an increase in benthic foraminiferal Mn/Ca for the same samples (Pearson correlation coefficient $r = 0.8$) with the five deepest samples having Mn/Ca >100 μmol/mol (highest value 235 μmol/mol). This suggests that Mn-$CaCO_3$ overgrowths were not fully removed in the cleaning steps and authigenic Cd may have elevated the Cd/Ca and CdW estimates (Boyle, 1983). CdW estimates from the deep Blake Outer Ridge cores are similar to those from the few other cores from similar depths and latitudes (Boyle, 1992; Marchitto & Broecker, 2006), and so we include all these data in the section and in our inversions, but the elevated Mn/Ca hint that some of the deep (> ~3,000-m) CdW estimates in the glacial North Atlantic estimated here and previously from Cd/Ca may be too high. Overall, inclusion of the new Blake Outer Ridge data elevates the average CdW value in the deep North Atlantic (>3,000 m) by only ~0.04 nmol/kg.

4.3. Glacial $\delta^{13}C_{AS}$

Consistent with previous inferences (Makou et al., 2010; Marchitto & Broecker, 2006; Oppo & Horowitz, 2000; Oppo & Lehman, 1993), glacial $\delta^{13}C_{AS}$ estimates suggest higher values than today in the North Atlantic and lower values in the shallow South Atlantic. Note that there is little paired data from the deep western South Atlantic to directly constrain glacial $\delta^{13}C_{AS}$ there; results of the inversion, which determine the color contouring, will be discussed in section 5.

Our compilation, which includes more data from the South Atlantic (Makou et al., 2010) and new data from the Demerara Rise and Blake Outer Ridge, however, for the first time clearly traces relatively low values from the shallow subtropical South Atlantic into the subtropical North Atlantic and portrays a coherent, layered distribution of upper Atlantic $\delta^{13}C_{AS}$, and hence upper water mass distribution. The $\delta^{13}C_{AS}$ data are consistent with previous inferences that AAIW reached the western tropical North Atlantic during the LGM (e.g., Huang et al., 2014; Poggemann et al., 2017).

The lower $\delta^{13}C_{AS}$ values in the South Atlantic at AAIW depths compared to modern suggest reduced air-sea gas exchange in the AAIW formation regions. High $\delta^{13}C_{AS}$ values in glacial NADW and subsurface water sourced from the northern subtropics (Figures 5c and 5f) suggest that the surface source waters were in contact with the atmosphere long enough to acquire the high air-sea gas exchange signature of relatively cold surface waters (e.g., Sigman et al., 2003).

4.4. Glacial B/Ca Data

Although exhibiting scatter, Demerera Rise glacial *C. pachyderma* B/Ca values are consistently higher than core top values and suggest $\Delta [CO_3^{=}]$ ranging from ~60–100 μmol/kg in cores between ~375 and 1,100 m, significantly higher than $\Delta[CO_3^{=}]$ at these water depths in the modern ocean (25–40 μmol/kg; Figure 2). These glacial estimates are similar to values in the modern subtropical North Atlantic lower thermocline and upper NADW (Figure S13 in the supporting information) and to values estimated for the shallow (<2-km) subpolar North Atlantic during the LGM (Yu et al., 2008). The single *C. wuellerstorfi* point from ~2,500 m suggests $\Delta [CO_3^{=}]$ similar to modern at this depth. Although *Uvigerina* B/Ca is less sensitive to $\Delta [CO_3^{=}]$ (Doss et al., 2018; Yu & Elderfield, 2007), where data are available, shallow glacial values are all higher than core top values, also suggesting higher glacial $\Delta [CO_3^{=}]$ (Figure S16 in the supporting information) in the upper water column. Higher preformed $[CO_3^{=}]$ due to lower atmospheric carbon dioxide levels likely contributed to the higher saturation state of the upper Atlantic during the LGM (Yu et al., 2010). However, given the Cd/Ca evidence for lower glacial phosphate, it is likely that a decrease in the accumulation of respired carbon also contributed to higher $\Delta [CO_3^{=}]$ in the tropical phosphate maximum.

5. Glacial Solution

The new glacial solution reproduces horizontal and vertical property gradients (Figure 5), with a few systematic misfits: CdW is lower than foraminifera-based estimates at ~1,000 and 2,500 m in the South Atlantic, and $\delta^{13}C_{AS}$ is lower than foraminifera-based estimates at ~2,500 m (Figure 5c). While there are no paired $\delta^{13}C$ and

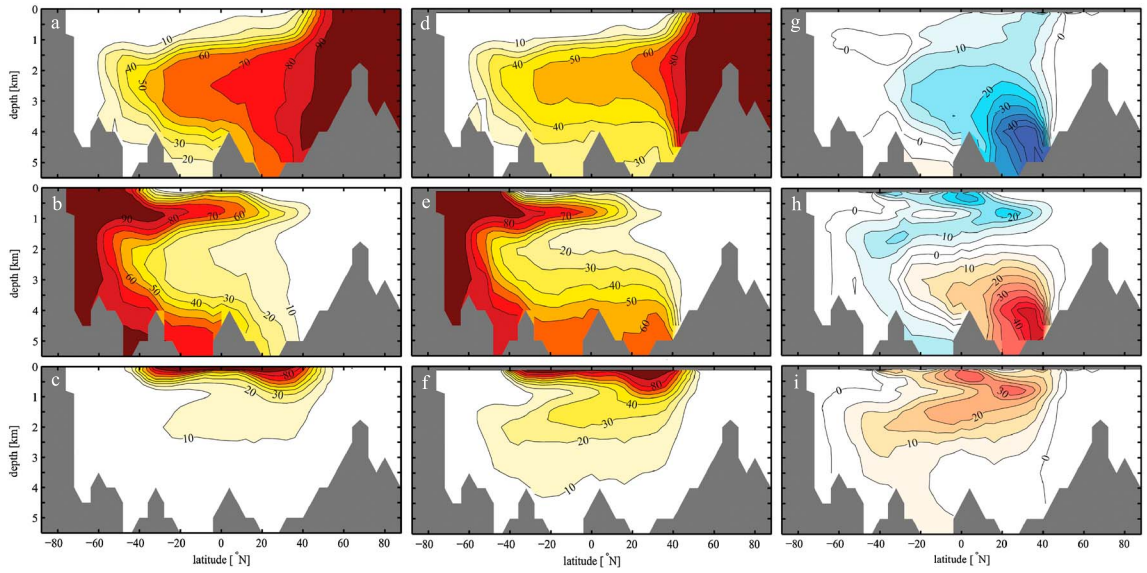

Figure 6. (a–c) Modern and (d–f) glacial solutions of the percentage of water deriving from high-latitude North Atlantic (top), Antarctic and sub-Antarctic (middle), and subtropical sources (bottom), along the western Atlantic GEOSECS transect. Panels (e)–(g) are their glacial-modern differences, respectively. Results in all panels are expressed as a percentage of water from the three sources. Panel (a) from Gebbie (2014).

CdW from the deep western South Atlantic (>2,500 m), the solution derives information to reconstruct $\delta^{13}C_{AS}$ values there from the unpaired data, from deep eastern South Atlantic data (Figure S14 in the supporting information), and from deep North Atlantic data. Notably, glacial $\delta^{13}C_{AS}$ estimates are higher in the North than South Atlantic, opposite to today (Charles et al., 1993; Figures 5c and 5f).

The solution does not reproduce the $\delta^{13}C$ value as low as measured in our shallowest Demerara Rise core (Figure 5a), because $\delta^{13}C$ values measured in the nearest Demerara Rise core, as well as in the nearby surface, are higher. Nearby CdW estimates also suggest that $\delta^{13}C$ was not as low as measured in the shallowest Demerara Rise core, unless $\delta^{13}C_{AS}$ was also low in an isolated region around the core site. These, and other smaller misfits, are more pronounced in comparisons of LGM-Holocene differences (Figures 5d and 5e). A large horizontal gradient is supported across the Greenland-Iceland-Scotland Ridge, although there is only one benthic (*C. wuellerstorfi*) $\delta^{18}O$ and $\delta^{13}C$ value each to constrain the solution there (Bauch et al., 2001). The glacial-modern $\delta^{18}O$ difference (~0.3‰) is much less than the typical difference just south of the sills (~1.7‰), likely giving rise to the large property gradients. A bathymetric constraint also exists but is not apparent in the Western Atlantic section because the deepest water column at each latitude is used to map the bathymetry.

5.1. Glacial-Modern Water Mass Fraction Changes

The glacial solution suggests changes in the distribution of NADW, SOW, and subtropical waters compared to modern (Figure 6). As in a previous solution (Gebbie, 2014), in the deep North Atlantic, there is a decrease in the NADW fraction and an increase in the SOW fraction. The increase in the SOW fraction likely results from the much lower $\delta^{13}C_{AS}$ values at depth than in shallow North Atlantic (Figure 5). If deep glacial CdW and/or $\delta^{13}C$ estimates contain a calibration bias, for example, underestimate $\delta^{13}C_{AS}$ in the deep North Atlantic, then the SOW fraction is overestimated there.

The new solution further suggests that waters forming south of the modern-day North Atlantic subpolar front partially replaced northern source waters that form farther north in the modern day (Figure 6i). The depth of the core of these combined high-latitude and subtropical source waters filling the western Atlantic from the north can be approximated by the depth of the minimum percentage of high-latitude SOW (Figure 6e) and deepens from ~1,500 m in the North Atlantic to ~2,000 m in the South Atlantic, or ~500 m shallower than modern (Figure 6). The reduction in the fraction of SOW centered at ~1,500 m and 30°S (Figure 6h) indicates that the combined northern source water masses comprised a greater fraction of the water masses in the

shallow South Atlantic than in the modern. The decrease in the fraction of SOW in the South Atlantic below ~4,000 m is due to the flattening of the isopleths of water mass fractions (the %SOW/NADW contours) in the solution.

The glacial solution is thus consistent with the prevailing view that during the LGM, SOW partially replaced NADW at depth and that the core of NADW shoaled (e.g., Boyle & Keigwin, 1987; Curry & Oppo, 2005). Our results suggest a similar fraction of northern source water throughout the glacial Atlantic below 3,000 m as a recent study based on neodymium isotopes (Howe et al., 2016). Our solution, however, distinguishes between waters forming north and south of the modern-day North Atlantic subpolar front and moreover solves for changes in water mass fractions shallower than 1,000 m.

The glacial solution suggests much lower CdW values and higher $\delta^{13}C_{AS}$ values in the Nordic Seas than in the open North Atlantic. Regardless of whether these values are correct (there are no Cd/Ca data to constrain them), the solution suggests a reduced influence of waters from the Nordic Seas in the western Atlantic south of the sills, consistent with previous work suggesting that northern source waters to the western Atlantic formed south of the sills (Labeyrie et al., 1992). Additional benthic $\delta^{13}C$, Cd/Ca, and $\delta^{18}O$ data from the Nordic Seas are required to confirm this inference, however.

The fraction of SOW is lower than modern between 1,000 and 2,000 m throughout the South Atlantic and equatorial region (Figure 6h). The fraction of NADW is also lower at these depths (Figure 6g), and both decreases are compensated for by an increase in the fraction of waters sourced from the area of the modern northern subtropics (Figure 6i). These water mass fraction changes are consistent with a greater influence of a shallower glacial northern source (e.g., Boyle & Keigwin, 1987) and better ventilation of the deep subtropical North Atlantic thermocline (Slowey & Curry, 1992).

The glacial solution suggests a reduction in the fraction of AAIW in the western tropical North Atlantic; for example, at 20°N, the contribution is reduced from ~40% in the modern ocean to ~20% in the glacial solution (Figures 6b and 6e). The results suggest a similar decrease in the fraction of AAIW at the Demerara Rise (~8°N), contrasting with neodymium isotope data, which at face value suggest a higher fraction of AAIW in the shallow tropics during the LGM (Huang et al., 2014). However, interpretation of neodymium isotopes at this location may be complicated by possible end-member changes (Huang et al., 2014; Xie et al., 2014), boundary exchange (e.g., Howe et al., 2018), and/or by changes in the contribution of the radiogenic signature from the Caribbean Sea (Gu et al., 2017).

5.2. Glacial-Modern Water Mass Property Changes

In the modern, phosphate is lowest in the surface and thermocline of the subtropical gyres (Figure S5 in the supporting information). While this is also the case in the glacial solution, like CdW (Figures 5b and 5e) on which it is based, low phosphate extends deeper in the subtropical gyres of both hemispheres, especially in the North Atlantic (Figures 7a and 7b) where nutrient-depleted subtropical waters make up a greater fraction relative to high-latitude northern and southern source waters (Figures 6g–6i). The results further suggest that phosphate was lower throughout the Atlantic above 2 km (Figure 7b), with the greatest reduction occurring in the subtropical South Atlantic thermocline and AAIW and extending into the tropical North Atlantic at modern AAIW depths. The increase in the deep North Atlantic (Figure 7d) corresponds to the region with the greatest replacement of modern NADW by SOW (Figure 6e). The observations confirm nutrient deepening in the glacial Atlantic (Boyle, 1988b).

The glacial solution separates phosphate and $\delta^{13}C$ changes into preformed and remineralized components, providing insight into why the spatial patterns of $\delta^{13}C$, CdW, and $\delta^{13}C_{AS}$ glacial-interglacial differences diverge from each other (Figures 5d and 5e). Preformed phosphate generally decreases more than remineralized phosphate in the upper ocean, except in the very shallow northern tropics, where remineralized phosphate decreases more (Figures 7e and 7f). These differences result in small changes in the remineralized-to-total phosphate ratios, although the glacial pattern is similar to modern (Figures S10 and S18 in the supporting information).

5.2.1. Distribution of Preformed Phosphate and $\delta^{13}C$

The pattern of preformed phosphate closely resembles that of total phosphate, with lowest preformed phosphate in the subtropical thermoclines of both hemispheres and in the shallow subpolar North Atlantic. Like total phosphate, the difference from modern is especially pronounced in the subtropical South Atlantic

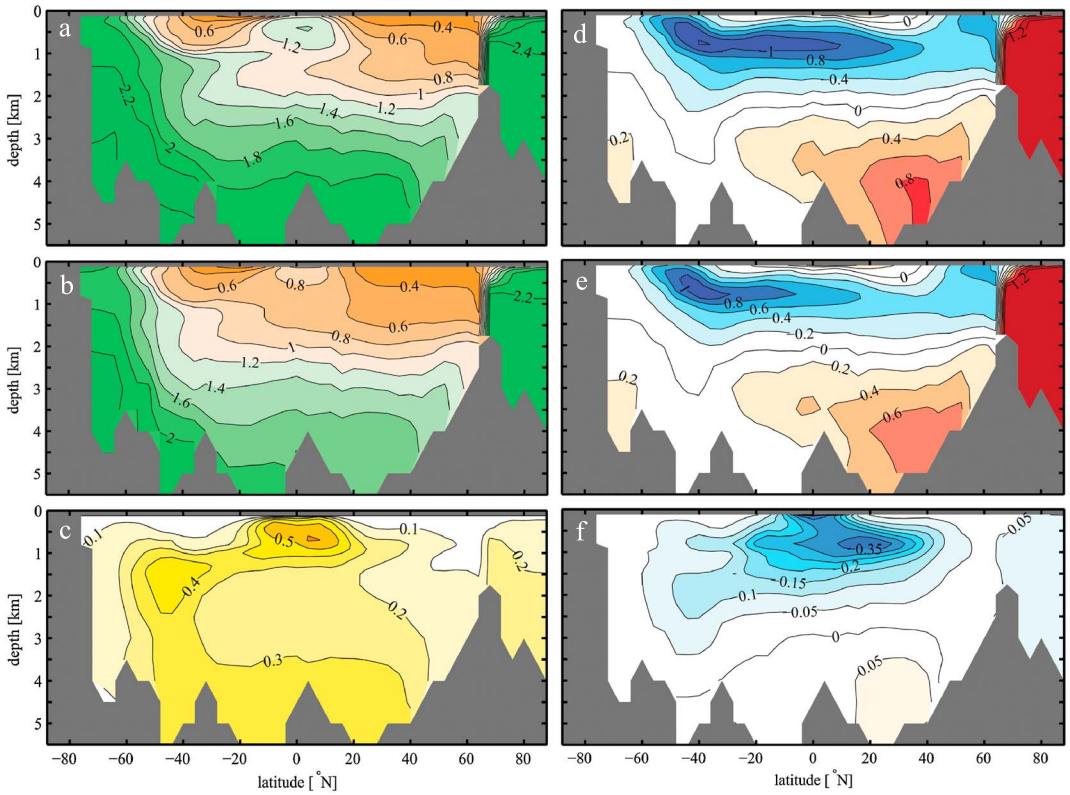

Figure 7. Glacial solution of (a) phosphate, (b) preformed phosphate and (c) remineralized phosphate along the western Atlantic GEOSECS transect, and (d–f) glacial-modern differences, respectively.

thermocline and AAIW (Figure 7e) and low preformed values extend deeper in the North than South Atlantic, likewise reflecting the sinking and southward flow of nutrient-depleted NADW (Figure 7b). Compared to modern, northern source waters have lower performed nutrients (Figures 7c and 7d) and higher preformed $\delta^{13}C$ (Figures 8a and 8b), and the opposite is true of deep SOW. The phosphate increase in the deep North Atlantic is attributed to preformed phosphate, corresponding to the increase in SOW. The results suggest that both preformed phosphate and preformed $\delta^{13}C$ were lower in glacial AAIW, giving rise to the large reduction in glacial $\delta^{13}C_{AS}$ values (Figure 5).

5.2.2. Distribution of Remineralized Phosphate

The spatial pattern of inferred glacial remineralized phosphate (Figure 7c) is similar to modern (Figure S8 in the supporting information), with lower concentrations in the subsurface North than South Atlantic and highest values at ~1–2 km in the South Atlantic and especially in the shallow tropics (Figure 7f). Relatively low remineralized phosphate (<0.3 μmol/kg) in the glacial solution approximately coincides with the tongue of northern source waters (e.g., <40% high-latitude SOW; Figure 6b), suggesting that it was still relatively well ventilated compared to southern sources.

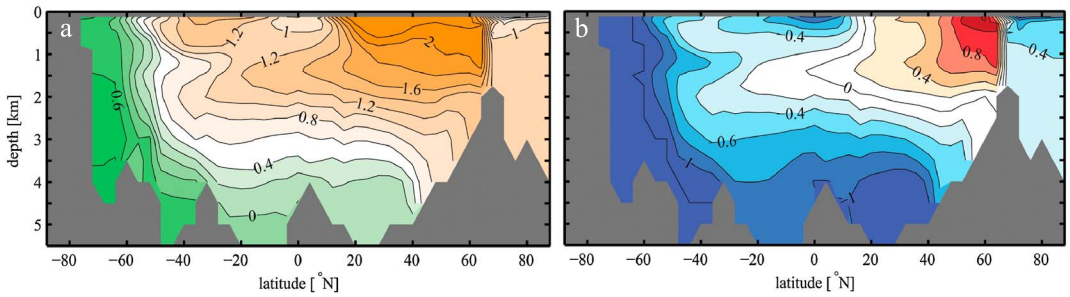

Figure 8. Glacial reconstruction of preformed (a) $\delta^{13}C$ and the (b) the glacial-modern difference.

Remineralized phosphate decreases everywhere that nutrient-depleted North Atlantic subtropical thermocline water partially replaced relatively nutrient-rich southern sourced water (Figures 6h, 6i, and 7f). The decrease is centered at ~20°N on the northern edge of the North Atlantic phosphate maximum (see Figure S5 in the supporting information), extends northward to ~40°N, southward to the center of the modern tropical phosphate maximum, into the subtropical south Atlantic, and as deep as ~2 km (Figure 7f). There is also a slight increase in remineralized phosphate in the deep North Atlantic.

The spatial pattern of changes in remineralized phosphate is consistent with a decrease in accumulated respired carbon inferred from B/Ca data at the Demerara Rise (Figure 2) and other areas such as the shallow North Atlantic (e.g., Yu et al., 2010) and middepth (~2,000 m) South Atlantic (Lacerra et al., 2017). The inferred pattern is also consistent with little or no change at ~2,500 m on the Demerara Rise (Figure 2) and a small increase in the deep North Atlantic (e.g., Yu et al., 2010).

5.2.3. Comparison to Previous Solutions

Similar to other estimates using paleoceanographic data to constrain subsurface Atlantic water masses and properties, the new results suggest shoaling of the NADW core by about 500 m (Gebbie, 2014; Kurahashi-Nakamura et al., 2017). These previous studies do not diagnose changes in the fraction of shallow high-latitude SOW or subtropical waters. Our solution suggests a much greater reduction in the fraction of high-latitude NADW than either of these previous studies. Kurahashi-Nakamura et al. (2017) use different methods and subsurface data from below 1,000 m. Differences from Gebbie (2014) likely arise from adding more Cd/Ca, $\delta^{13}C$, and $\delta^{18}O$ data, surface water $\delta^{13}C_{DIC}$ constraints, and new Cd distribution coefficients. As a result of a higher SOW fraction at depth in this solution compared to Gebbie (2014), more of the deep Atlantic phosphate increase is attributed to an increase in preformed rather than remineralized phosphate.

5.2.4. AAIW and the Tropical Phosphate Maximum

In the high-latitude South Atlantic, reduced preformed phosphate contributes more than reduced respired phosphate to the lower glacial phosphate values (Figures 7e and 7f). In the inversion, southeastern Pacific surface and thermocline waters, where AAIW forms today (Talley, 1999), are significantly more phosphate depleted than modern (not shown). Moreover, phosphate is also lower off the east of the southern tip of South America where mixing also influences the properties of AAIW (Talley, 1999). Thus, a possible explanation for the low nutrients in glacial AAIW is that its source waters were more nutrient depleted, consistent with paleoceanographic evidence (François et al., 1997; Robinson & Sigman, 2008; Sigman et al., 2003; Sigman & Boyle, 2000). Lower preformed nutrients in shallow glacial NADW (Figure 7e) may also have contributed to lowering preformed nutrients in AAIW, which is in part sourced by NADW (Marshall & Speer, 2012; Poggemann et al., 2017).

The glacial solution suggests that at least two factors contributed to lower nutrients in the region of the modern shallow tropical Atlantic phosphate maximum. First, a reduction in remineralized phosphate occurred everywhere that nutrient-depleted North Atlantic subtropical thermocline water partially replaced relatively nutrient-rich southern sourced water above 2 km (Figures 6h, 6i, and 7f). The greatest replacement of nutrient-rich AAIW with North Atlantic subtropical waters occurs at the northern edge of modern AAIW (Figures 6e and 6f), resulting in the largest decrease in remineralized phosphate in the core of today's phosphate maximum. Second, preformed phosphate was lower in glacial AAIW than in the modern ocean, contributing to lower phosphate along its northward flow path and within the tropical phosphate maximum.

Radiocarbon data may imply a shorter residence time in the shallow tropics (Freeman et al., 2016), and colder waters may have reduced remineralization rates (Matsumoto, 2007). We cannot rule out that factors such as faster flow or reduced remineralization rate (e.g., vertical flux) contributed to the weaker glacial phosphate maximum, as the local source of respired nutrients, which is a product of the remineralization rate (e.g., vertical flux) and residence time of water, is assumed nearly identical to modern in each grid cell.

The evidence that all water mass sources to the upper western tropical Atlantic were characterized by relatively low preformed phosphate is consistent with the hypothesis that lower nutrient supply in waters upwelling in the western tropical Atlantic contributed to lower biological productivity and reduced the supply of organic material to the subsurface (Sigman & Boyle, 2000). If productivity were, in fact, reduced due to a lower nutrient supply, this would have resulted in a positive feedback that would have further reduced the intensity of the phosphate maximum. However, we cannot diagnose such changes with the inversion. Instead, our results suggesting that changes in circulation contributed to lower remineralized phosphate in the area of

the modern tropical phosphate maximum may imply better oxygenation of the upper Atlantic, enhancing the effect of higher solubility at colder temperatures and extending evidence for better oxygenation of the intermediate-depth Indo-Pacific (Galbraith & Jaccard, 2015; Jaccard & Galbraith, 2012) into the Atlantic Ocean.

6. Implications for the AMOC and Atmospheric CO_2

Given AAIW's role as a supplier of NADW that is exported at depth (Rintoul, 1991; Schmitz & McCartney, 1993), the finding of weaker AAIW influence in the northern tropics appears consistent with an overall weaker AMOC (Gu et al., 2017), regardless of whether (e.g., Gherardi et al., 2005; Lippold et al., 2016; McManus et al., 2004) or not (Lynch-Stieglitz et al., 1999, 2006) shallow overturning was more vigorous than today's. There are, however, other possibilities. For example, the supply of AAIW to the northern subtropics may have been the same as modern, but the supply of northern source waters to AAIW depths increased more, reducing the fraction of AAIW in the water mass mixture. If the AMOC was as strong as the modern, this scenario would require a greater role of surface and thermocline water flowing northward to balance deep NADW export. This hypothesis cannot be tested with the inversion, which does not explicitly solve for circulation rates in the surface and thermocline. Another possibility is that consistent with overall stronger glacial winds, more AAIW upwelled in the tropics, joining northward flowing surface and thermocline water to balance deep NADW export. However, given that AAIW within the South Atlantic appears to have had about the same concentration of dissolved silica as modern (e.g., Hendry et al., 2012), and there is no evidence for enhanced opal production in the tropical Atlantic upwelling regions during the LGM (e.g., Meckler et al., 2013), this scenario seems unlikely.

Visually, the spatial distributions of glacial-modern differences in $\delta^{13}C$ and phosphate (Figures 6 and 7) are most similar to the *weak NADW and very weak AABW* scenario favored by Menviel et al. (2017). The spatial patterns of remineralized material are also similar (remineralized carbon in their case, remineralized phosphate in this study). These similarities are not unexpected, as there is some overlap in the underlying data: benthic $\delta^{13}C$ is used in both studies. On the other hand, another recent study that combined an ocean general circulation model with glacial data arrived at the opposite conclusion that the glacial AMOC was stronger than modern (Kurahashi-Nakamura et al., 2017). However, in that study, subsurface data from sites shallower than 1,000 m were excluded, and it is unclear if the model was fully equilibrated or whether the stronger AMOC is a transient effect as seen in simpler models (Jansen & Nadeau, 2016). With these caveats, it seems so far possible to match a subset of glacial data with either a weaker (e.g., Menviel et al., 2017) or stronger (e.g., Kurahashi-Nakamura et al., 2017) AMOC. Studies that assimilate the combined glacial data used in these analyses, including our own, and more surface constraints, may converge on a solution for rates of water exchange between grid cells, and hence AMOC strength.

Previous work suggested that high preformed $\delta^{13}C$ and low preformed phosphate in the shallow North Atlantic requires export of shallow NADW out of the Atlantic; the greater the import of relatively high-nutrient AAIW into the Atlantic, the greater export is required to maintain low phosphate (Sigman et al., 2003). Our glacial solution suggests that in the South Atlantic at ~2,000 m, the fraction of combined northern source waters was greater than modern and northern source waters extended at least as far south as modern (Figure 6e), consistent with glacial NADW export (e.g., Lynch-Stieglitz et al., 1996). Our results are thus consistent with the hypothesis that shallow NADW export combined with reduced AAIW import (or more precisely, a smaller water mass fraction of AAIW in the North Atlantic) contributed to glacial upper Atlantic nutrient depletion. Moreover, AAIW was not as enriched in nutrients as the modern, and the phosphate gradient between NADW and AAIW was smaller than today (Figures 7a, 7b, and S5 in the supporting information), requiring less NADW export to balance a given AAIW import. Thus, the finding that AAIW was relatively nutrient depleted may suggest a more closed circulation between glacial AAIW and NADW than exists today (e.g., Ferrari et al., 2014; Poggemann et al., 2017).

However, atmospheric CO_2 considerations favor greater volume of NADW in the glacial ocean. Previous studies suggest that lower glacial atmospheric CO_2 requires ventilation of the global ocean with a higher fraction of waters having higher remineralized to total phosphate ratios than today or, more generally, with lower preformed phosphate than today (e.g., Ito & Follows, 2005; Kwon et al., 2012). In our glacial scenario, preformed phosphate decreases (and the remineralized to total phosphate ratio increases) in North

Atlantic waters that originate at the surface between 40 and 60°N. As these waters sink to fill the middepth Atlantic (Figure 6d), they mix with waters originating north of the Greenland-Iceland-Scotland Ridge, which, in the glacial inversion, have both very high preformed values and very low remineralized to total phosphate ratios. Mixing with these waters increases the preformed values so that there is almost no net glacial-modern change in preformed phosphate (Figure 7e) or in the remineralized to total phosphate ratio (Figure S18 in the supporting information), in the core of glacial NADW (~1,500–2,500-m depth). The reconstructed pattern of the ratio of remineralized phosphate to total phosphate is similar to the modern (Figure S10 in the supporting information) with small (up to 0.05) increases and decreases above and below 1,500 m, respectively (Figure S18 in the supporting information) implying that changes in subsurface water masses within the Atlantic resulted in little change in the efficiency of the soft tissue pump (Ito & Follows, 2005). Given that there is almost no data constraining Nordic Sea properties, it is possible that preformed phosphate in the core of glacial NADW was lower than estimated here and contributed to a more efficient soft tissue pump during glacial times.

Whether or not glacial NADW had lower preformed phosphate than estimated here, its preformed values were likely still lower than the Pacific, so if there was a greater fraction of NADW in the global ocean, it would have contributed to a more efficient soft tissue pump and to lower atmospheric CO_2 (Kwon et al., 2012). Alternatively, if SOW filling the global deep ocean had lower preformed phosphate than estimated for the Atlantic here, perhaps by a SOW mass that was distinct from that ventilating the deep Atlantic (e.g., Sikes et al., 2017), it could have contributed to a stronger biologic pump. If AAIW filling the other basins also had lower preformed phosphate than modern, like Atlantic AAIW, it may have also played a role. These scenarios should be evaluated in the future by including Indo-Pacific data in an inversion.

7. Summary and Conclusions

An inversion of glacial data confirms that the core of NADW was ~500 m shallower than modern and further suggests that NADW contained a higher fraction of water formed south of the modern North Atlantic subpolar front at the expense of decreases in both higher-latitude NADW and AAIW. The NADW core extended at least as far south as modern, consistent with glacial NADW export (e.g., Lynch-Stieglitz et al., 1996).

Benthic Cd/Ca data suggest that phosphate was lower than modern above 2,500 m throughout the Atlantic and higher below 2,500 m. Our glacial solution suggests that the higher glacial deep phosphate is due to the partial replacement of NADW by SOW, having higher preformed phosphate (Figure 7e), rather than to an increase in respired carbon, as suggested recently (Freeman et al., 2016; Hoogakker et al., 2014; Howe et al., 2016). This is in part because in our solution, low glacial $\delta^{13}C$ values in SOW in the deep Atlantic are attributed to lower preformed $\delta^{13}C$ (and $\delta^{13}C_{AS}$) values.

The greatest phosphate decrease occurred in the subtropical South Atlantic thermocline and AAIW, where glacial preformed phosphate was much lower than modern. Reduced regenerated phosphate also contributed to lower glacial phosphate above ~2,500 m, especially in the tropical phosphate maximum. Both an increase in the fraction of nutrient-depleted North Atlantic subtropical thermocline water relative to AAIW and lower preformed phosphate in AAIW contributed to reduced phosphate in the shallow tropical Atlantic. New benthic B/Ca data from the shallow tropics suggest significantly higher $\Delta[CO_3^{=}]$ than in the modern ocean, likely the result of an associated decrease in the accumulation of respired carbon, and higher preformed $[CO_3^{=}]$ due to lower atmospheric carbon dioxide levels (Yu et al., 2010). The relatively small benthic $\delta^{13}C$ change in the shallow phosphate maximum relative to Cd/Ca and B/Ca largely reflects lower $\delta^{13}C_{AS}$ in glacial AAIW.

As AAIW is the main source of nutrients to the modern North Atlantic (Sarmiento et al., 2004; Tuerena et al., 2015), a decrease in its glacial extent and nutrient content would have contributed to the lower nutrients in glacial NADW and likely to reduced low-latitude biological productivity. Better upper ocean oxygenation is also implied by the evidence for less accumulation of respired nutrients, enhancing the effect of greater solubility at colder temperatures.

As the phosphate gradient between NADW and AAIW was smaller than today, less NADW export may have been required to balance a given AAIW import and also maintain the low nutrients in the upper ocean, perhaps implying a more closed circulation between glacial AAIW and NADW, as suggested in several recent

studies (e.g., Ferrari et al., 2014; Poggemann et al., 2017). However, one way to reconcile the small changes in preformed nutrients in NADW implied by the inversion with lower atmospheric pCO_2 is for glacial NADW, whose preformed phosphate was presumably still lower than that of the Indian and Pacific Oceans, to make up a larger fraction of the water mass mixture in the global ocean (Kwon et al., 2012). In addition, due to weak constraints on Nordic Sea properties, we may have overestimated the preformed phosphate concentration of glacial NADW.

7.1. Uncertainties and Outlook

Our inversion took advantage of published data compilations (Curry & Oppo, 2005; Marchitto & Broecker, 2006) and, as a result, included little benthic $\delta^{18}O$ data from the eastern Atlantic (Figure S14 in the supporting information). Moreover, the lack of benthic Cd/Ca data and very sparse $\delta^{18}O$ and $\delta^{13}C$ data from the Nordic Seas may have biased the properties of NADW formed in the high latitudes.

Our Cd calibration does not take into account the possible influence of lower glacial carbonate saturation state in the deep Atlantic (Yu et al., 2008) on lowering the Cd distribution coefficient (Marchitto et al., 2000; McCorkle et al., 1995). While this effect is only apparent at very low saturation states, lack of consideration of this effect might have underestimated glacial CdW and hence $\delta^{13}C_{AS}$ at depth. If deep Atlantic $\delta^{13}C_{AS}$ values were higher than estimated, then the reduction in the NADW fraction at depth may have been smaller than reconstructed, and more of the (larger) phosphate increase at depth may have been attributed to remineralized phosphate. Eventually, as the coverage of quantitative glacial saturation state estimates increases, and as the effect of saturation state on the Cd distribution coefficient for each species is quantified better, this information can be included in future work. On the other hand, higher Mn/Ca ratios with increasing water depth at the Blake Outer Ridge (section 4.3) may indicate that glacial deep North Atlantic CdW estimates are too high, opposite the effect of carbonate saturation state on CdW estimates. It is also possible that the relationship between subsurface seawater Cd and phosphate changed in the past (e.g., Middag et al., 2018). Offsets between $\delta^{13}C$ of benthic foraminifera and seawater are not well understood, and so no attempt was made to correct for core top offsets. Incorrect estimates of past $\delta^{13}C_{DIC}$ would also influence the solution.

The glacial solution does not resolve the lowest benthic $\delta^{13}C$ value on the shallow Demerara Rise (Figure 5b), likely because there is only one data point and the solution simultaneously fits nearby higher $\delta^{13}C$ values and relatively low CdW estimates. While it is thus possible that the intensity of the phosphate maximum relative to the source waters is similar to modern, the good fit of the inversion to the surrounding data points (Figure 5) suggests that at the very least, the phosphate maximum had a smaller spatial extent than modern.

Improvements could also be made in the inversion itself. In addition to adding data that might help constrain absolute rates of water exchange between grid cells and hence the AMOC rate (e.g., radiocarbon data), the inversion could enforce reasonable air-sea fluxes, such as those produced from coupled climate models. This would permit explicitly closing the upper branch of the circulation in the mixed layer and provide, for example, more complete insights into changes in upwelling and northward flow. Including paired Cd/Ca and $\delta^{13}C$ data from well-dated glacial sediments from the Indian and Pacific Oceans might be useful for evaluating the hypothesis that more of the ocean was filled with NADW having low preformed phosphate, in essence corresponding to a strong biologic pump, and contributing to lower atmospheric CO_2 during glacial times (Hain et al., 2010; Kwon et al., 2012).

Acknowledgments
We thank the crew of R/V Knorr cruise 197-3, M. Jeglinski for laboratory assistance, and O. Marchal and S. Jaccard for helpful discussions and comments on the manuscript. Detailed, constructive comments from two reviewers also improved the manuscript. We are grateful for the rapid turnaround of our radiocarbon samples at the National Ocean Sciences Accelerator Mass Spectrometry facilities at WHOI. This work was funded by NSF grants OCE-0750880 (D. O. and W. C.), OCE-1335191 (D. O.), OCE-1558341 (D. O.), OCE-1536380 (G. G.); WHOI's Joint Initiative Awards Fund from the Andrew W. Mellon Foundation (D. O. and G. G.); a Columbus O'Donnell Iselin Senior Scientist Chair; and The Investment in Science Fund at WHOI. The Knorr 159 and 140 sediment cores are archived in the Sea Floor Samples Laboratory at WHOI. The authors declare no financial conflicts of interests. All supporting data will be archived at the NOAA/World Data Service for Paleoclimatology at the National Centers for Environmental Information (https://www.ncdc.noaa.gov/paleo/study/25010).

References

Adkins, J. F., McIntyre, K., & Schrag, D. P. (2002). The salinity, temperature, and delta ^{18}O of the glacial deep ocean. *Science*, *298*(5599), 1769–1773. https://doi.org/10.1126/science.1076252

Bainbridge, A. E. (1981, February 14). GEOSECS Atlantic expedition vol. 1. Hydrographic data, U. S. government printing office, Washington, DC. NSF. Retrieved fromhttp://epic.awi.de/34900/1/atlantic-expedition_vol1.pdf

Bauch, H. A., Spielhagen, R. F., Struck, U., Matthiessen, J., Thiede, J., & Heinemeier, J. (2001). A multiproxy reconstruction of the evolution of deep and surface waters in the subarctic Nordic seas over the last 30,000 years. *Quaternary Science Reviews*, *20*(4), 659–678. https://doi.org/10.1016/S0277-3791(00)00098-6

Belanger, P. E., Curry, W. B., & Matthews, R. K. (1981). Core-top evaluation of benthic foraminiferal isotopic ratios for paleo-oceanographic interpretations. *Palaeogeography, Palaeoclimatology, Palaeoecology*, *33*(1–3), 205–220. https://doi.org/10.1016/0031-0182(81)90039-0

Bemis, B. E., Spero, H. J., Bijma, J., & Lea, D. W. (1998). Reevaluation of the oxygen isotopic composition of planktonic foraminifera: Experimental results and revised paleotemperature equations. *Paleoceanography*, *13*, 150–160. https://doi.org/10.1029/98PA00070

Boyle, E. (1981). Cadmium, zinc, copper, and barium in foraminifera tests. *Earth and Planetary Science Letters*, *53*(1), 11–35. https://doi.org/10.1016/0012-821X(81)90022-4

Boyle, E. (1983). Manganese carbonate overgrowths on foraminifera tests. *Geochimica et Cosmochimica Acta*, *47*(10), 1815–1819. https://doi.org/10.1016/0016-7037(83)90029-7

Boyle, E. A. (1988a). Cadmium: Chemical tracer of deepwater paleoceanography. *Paleoceanography*, *3*, 471–489. https://doi.org/10.1029/PA003i004p00471

Boyle, E. A. (1988b). The role of vertical chemical fractionation in controlling late Quaternary atmospheric carbon dioxide. *Journal of Geophysical Research*, *93*, 15,701–15,714. https://doi.org/10.1029/JC093iC12p15701

Boyle, E. A. (1992). Cadmium and $\delta^{13}C$ paleochemical distributions durng the stage 2 glacial maximum. *Annual Reviews Planetary Science*, *20*(1), 245–287. https://doi.org/10.1146/annurev.ea.20.050192.001333

Boyle, E. A., & Keigwin, L. (1987). North Atlantic thermohaline circulation during the past 20,000 years linked to high-latitude surface temperature. *Nature*, *330*(6143), 35–40. https://doi.org/10.1038/330035a0

Boyle, E. A., & Keigwin, L. D. (1985). Comparison of Atlantic and Pacific paleochemical records for the last 215,000 years: Changes in deep ocean circulation and chemical inventories. *Earth and Planetary Science Letters*, *76*(1–2), 135–150. https://doi.org/10.1016/0012-821X(85)90154-2

Broecker, W. S., & Maier-Reimer, E. (1992). The influence of air and sea exchange on the carbon isotope distribution in the sea. *Global Biogeochemical Cycles*, *6*, 315–320. https://doi.org/10.1029/92GB01672

Brownlee, K. A. (1965). *Statistical Theory and Methodology in Science and Engineering*. New York: John Wiley.

Bryan, S. P., & Marchitto, T. M. (2010). Testing the utility of paleonutrient proxies Cd/Ca and Zn/Ca in benthic foraminifera from thermocline waters. *Geochemistry, Geophysics, Geosystems*, *11*, Q01005. https://doi.org/10.1029/2009gc002780

Burckel, P., Waelbroeck, C., Gherardi, J. M., Pichat, S., Arz, H., Lippold, J., et al. (2015). Atlantic Ocean circulation changes preceded millennial tropical South America rainfall events during the last glacial. *Geophysical Research Letters*, *42*, 411–418. https://doi.org/10.1002/2014GL062512

Burke, A., Marchal, O., Bradtmiller, L. I., McManus, J. F., & François, R. (2011). Application of an inverse method to interpret $^{231}Pa/^{230}Th$ observations from marine sediments. *Paleoceanography*, *26*, PA1212. https://doi.org/10.1029/2010PA002022

Butzin, M., Prange, M., & Lohmann, G. (2005). Radiocarbon simulations for the glacial ocean: The effects of wind stress, Southern Ocean sea ice and Heinrich events. *Earth and Planetary Science Letters*, *235*(1–2), 45–61. https://doi.org/10.1016/j.epsl.2005.03.003

Charles, C. D., Wright, J. D., & Fairbanks, R. G. (1993). Thermodynamic influences on the marine carbon isotope record. *Paleoceanography*, *8*, 691–697. https://doi.org/10.1029/93PA01803

Curry, W. B., Duplessy, J. C., Labeyrie, L. D., & Shackleton, N. J. (1988). Changes in the distribution of $\delta^{13}C$ of deep water ΣCO_2 between the Last Glaciation and the Holocene. *Paleoceanography*, *3*, 317–341. https://doi.org/10.1029/PA003i003p00317

Curry, W. B., & Oppo, D. W. (1997). Synchronous, high-frequency oscillations in tropical sea surface temperatures and North Atlantic deep water production during the last glacial cycle. *Paleoceanography*, *12*, 1–14. https://doi.org/10.1029/96PA02413

Curry, W. B., & Oppo, D. W. (2005). Glacial water mass geometry and the distribution of $\delta^{13}C$ of ΣCO_2 in the western Atlantic Ocean. *Paleoceanography*, *20*, PA1017. https://doi.org/10.1029/2004PA001021

Doss, W., Marchitto, T. M., Eagle, R., Rashid, H., & Tripati, A. (2018). Deconvolving the saturation state and temperature controls on benthic foraminiferal Li/Ca, based on downcore paired B/Ca measurements and coretop compilation. *Geochimica et Cosmochimica Acta*, *236*, 297–314. https://doi.org/10.1016/j.gca.2018.02.029

Duplessy, J. C., Shackleton, N. J., Fairbanks, R. G., Labeyrie, L., Oppo, D., & Kallel, N. (1988). Deepwater source variations during the last climatic cycle and their impact on the global deepwater circulation. *Paleoceanography*, *3*, 343–360. https://doi.org/10.1029/PA003i003p00343

Duplessy, J. C., Shackleton, N. J., Matthews, R. K., Prell, W., Ruddiman, W. F., Caralp, M., et al. (1984). ^{13}C record of benthic foraminifera in the last interglacial ocean: Implications for the carbon cycle and the global deep water circulation. *Quaternary Research*, *21*(02), 225–243. https://doi.org/10.1016/0033-5894(84)90099-1

Dyez, K. A., Zahn, R., & Hall, I. R. (2014). Multicentennial Agulhas leakage variability and links to North Atlantic climate during the past 80,000-years. *Paleoceanography*, *29*, 1238–1248. https://doi.org/10.1002/2014PA002698

Elderfield, H., & Rickaby, R. E. M. (2000). Oceanic Cd/P ratio and nutrient utilization in the glacial Southern Ocean. *Nature*, *405*(6784), 305–310. https://doi.org/10.1038/35012507

Emiliani, C. (1955). Pleistocene Temperatures. *The Journal of Geology*, *63*(6), 538–578. https://doi.org/10.1086/626295

Ferrari, R., Jansen, M. F., Adkins, J. F., Burke, A., Stewart, A. L., & Thompson, A. F. (2014). Antarctic sea ice control on ocean circulation in present and glacial climates. *Proceedings of the National Academy of Sciences of the United States of America*, *111*(24), 8753–8758. https://doi.org/10.1073/pnas.1323922111

Fontanier, C., Mackensen, A., Jorissen, F. J., Anschutz, P., Licari, L., & Griveaud, C. (2006). Stable oxygen and carbon isotopes of live benthic foraminifera from the Bay of Biscay: Microhabitat impact and seasonal variability. *Marine Micropaleontology*, *58*(3), 159–183. https://doi.org/10.1016/j.marmicro.2005.09.004

François, R., Altabet, M., Yu, E. F., Sigman, D. M., Bacon, M. P., & Frank, et al. (1997). Contribution of Southern Ocean surface-water stratification to low atmospheric CO_2 concentrations during the last glacial period. *Nature*, *389*(6654), 929–935. https://doi.org/10.1038/40073

Freeman, E., Skinner, L. C., Tisserand, A., Dokken, T., Timmermann, A., Menviel, L., et al. (2015). An Atlantic–Pacific ventilation seesaw across the last deglaciation. *Earth and Planetary Science Letters*, *424*, 237–244. https://doi.org/10.1016/j.epsl.2015.05.032

Freeman, E., Skinner, L. C., Waelbroeck, C., & Hodell, D. (2016). Radiocarbon evidence for enhanced respired carbon storage in the Atlantic at the Last Glacial Maximum. *Nature Communications*, *7*(May), 11,998. https://doi.org/10.1038/ncomms11998

Galbraith, E. D., & Jaccard, S. L. (2015). Deglacial weakening of the oceanic soft tissue pump: Global constraints from sedimentary nitrogen isotopes and oxygenation proxies. *Quaternary Science Reviews*, *109*, 38–48. https://doi.org/10.1016/j.quascirev.2014.11.012

Gebbie, G. (2014). How much did glacial North Atlantic water shoal? *Paleoceanography*, *29*, 190–209. https://doi.org/10.1002/2013PA002557

Gebbie, G., Peterson, C. D., Lisiecki, L. E., & Spero, H. J. (2015). Global-mean marine $\delta^{13}C$ and its uncertainty in a glacial state estimate. *Quaternary Science Reviews*, *125*, 144–159. https://doi.org/10.1016/j.quascirev.2015.08.010

Gebbie, G., Streletz, G. J., & Spero, H. J. (2016). How well would modern-day oceanic property distributions be known with paleoceanographic-like observations? *Paleoceanography*, *31*, 472–490. https://doi.org/10.1002/2015PA002917

Gherardi, J.-M., Labeyrie, L., McManus, J. F., François, R., Skinner, L. C., & Cortijo, E. (2005). Evidence from the northeastern Atlantic basin for variability in the rate of the meridional overturning circulation through the last deglaciation. *Earth and Planetary Science Letters*, *240*(3–4), 710–723. https://doi.org/10.1016/j.epsl.2005.09.061

Gouretski, V. V., & Koltermann, K. P. (2004). WOCE Global Hydrographic Climatology. Berichte des Bundesamtes fur Seeschifffahrt und Hydrographie.

Gruber, N., & Sarmiento, J. L. (2002). Large-scale biogeochemical-physical interactions in elemental cycles. *The Sea*, *12*, 337–399.

Gu, S., Liu, Z., Zhang, J., Rempfer, J., Joos, J., Brady, E., et al. (2017). Coherent response of Antarctic Intermediate Water and Atlantic Meridional Overturning Circulation during the last deglaciation. *Paleoceanography*, *32*, 1036–1053. https://doi.org/10.1002/2017PA003092

Hain, M. P., Sigman, D. M., & Haug, G. H. (2010). Carbon dioxide effects of Antarctic stratification, North Atlantic Intermediate Water formation, and subantarctic nutrient drawdown during the last ice age: Diagnosis and synthesis in a geochemical box model. *Global Biogeochemical Cycles*, *24*, GB4023. https://doi.org/10.1029/2010GB003790

Hayes, C. T., Anderson, R. F., Fleisher, M. Q., Vivancos, S. M., Lam, P. J., Ohnemus, D. C., et al. (2015). Intensity of Th and Pa scavenging partitioned by particle chemistry in the North Atlantic Ocean. *Marine Chemistry*, *170*, 49–60. https://doi.org/10.1016/j.marchem.2015.01.006

Hendry, K. R., Robinson, L. F., Meredith, M. P., Mulitza, S., Chiessi, C. M., & Arz, H. (2012). Abrupt changes in high-latitude nutrient supply to the Atlantic during the last glacial cycle. *Geology*, *40*(2), 123–126. https://doi.org/10.1130/G32779.1

Hesse, T., Butzin, M., Bickert, T., & Lohmann, G. (2011). A model-data comparison of $\delta^{13}C$ in the glacial Atlantic Ocean. *Paleoceanography*, *26*, PA3220. https://doi.org/10.1029/2010PA002085

Hodell, D. A., Channell, J. E. T., Curtis, J. H., Romero, O. E., & Röhl, U. (2008). Onset of "Hudson Strait" Heinrich events in the eastern North Atlantic at the end of the middle Pleistocene transition (~640 ka). *Paleoceanography*, *23*, PA4218. https://doi.org/10.1029/2008PA001591

Hodell, D. A., Evans, H. F., Channell, J. E. T., & Curtis, J. H. (2010). Phase relationships of North Atlantic ice-rafted debris and surface-deep climate proxies during the last glacial period. *Quaternary Science Reviews*, *29*(27–28), 3875–3886. https://doi.org/10.1016/j.quascirev.2010.09.006

Hoffman, J. L., & Lund, D. C. (2012). Refining the stable isotope budget for Antarctic Bottom Water: New foraminiferal data from the abyssal southwest Atlantic. *Paleoceanography*, *27*, PA1213. https://doi.org/10.1029/2011PA002216

Hoogakker, B. A. A., Elderfield, H., Schmiedl, G., McCave, I. N., & Rickaby, R. E. M. (2014). Glacial–interglacial changes in bottom-water oxygen content on the Portuguese margin. *Nature Geoscience*, *8*(1), 40–43. https://doi.org/10.1038/ngeo2317

Howe, J. N. W., Huang, K.-F., Oppo, D. W., Chiessi, C. M., Mulitza, S., Blusztajn, J., et al. (2018). Similar mid-depth Atlantic water mass provenance during the last Glacial Maximum and Heinrich Stadial 1. *Earth and Planetary Science Letters*, *490*, 51–61. https://doi.org/10.1016/j.epsl.2018.03.006

Howe, J. N. W., Piotrowski, A. M., Noble, T. L., Mulitza, S., Chiessi, C. M., & Bayon, G. (2016). North Atlantic Deep Water production during the Last Glacial Maximum. *Nature Communications*, *7*, 11,765. https://doi.org/10.1038/ncomms11765

Huang, K. F., Oppo, D. W., & Curry, W. B. (2014). Decreased influence of Antarctic intermediate water in the tropical Atlantic during North Atlantic cold events. *Earth and Planetary Science Letters*, *389*, 200–208. https://doi.org/10.1016/j.epsl.2013.12.037

Huang, K.-F., You, C.-F., Lin, H.-L., & Shieh, Y.-T. (2008). In situ calibration of Mg/Ca ratio in planktonic foraminiferal shell using time series sediment trap: A case study of intense dissolution artifact in the South China Sea. *Geochemistry, Geophysics, Geosystems*, *9*, Q04016. https://doi.org/10.1029/2007GC001660

Ito, T., & Follows, M. J. (2005). Preformed phosphate, the soft tissue pump, and atmospheric CO_2. *Journal of Marine Research*, *63*(4), 813–839. https://doi.org/10.1357/0022240054663231

Jaccard, S. L., & Galbraith, E. D. (2012). Large climate-driven changes of oceanic oxygen concentrations during the last deglaciation. *Nature Geoscience*, *5*(2), 151–156. https://doi.org/10.1038/ngeo1352

Jansen, M. F., & Nadeau, L.-P. (2016). The effect of Southern Ocean surface buoyancy loss on the deep-ocean circulation and stratification. *Journal of Physical Oceanography*, *46*(11), 3455–3470. https://doi.org/10.1175/JPO-D-16-0084.1

Keigwin, L. D. (2004). Radiocarbon and stable isotope constraints on Last Glacial Maximum and Younger Dryas ventilation in the western North Atlantic. *Paleoceanography*, *19*, PA4012. https://doi.org/10.1029/2004PA001029

Keigwin, L. D., & Swift, S. A. (2017). Carbon isotope evidence for a northern source of deep water in the glacial western North Atlantic. *Proceedings of the National Academy of Sciences*, *114*(11), 2831–2835. https://doi.org/10.1073/pnas.1614693114

Key, R. M., Kozyr, A., Sabine, C. L., Lee, K., Wanninkhof, R., Bullister, J. L., et al. (2004). A global ocean carbon climatology: Results from Global Data Analysis Project (GLODAP). *Global Biogeochemical Cycles*, *18*, GB4031. https://doi.org/10.1029/2004GB002247

Kroopnick, P. M. (1985). The distribution of ^{13}C of ΣCO_2 in the world oceans. *Deep Sea Research Part A. Oceanographic Research Papers*, *32*(1), 57–84. https://doi.org/10.1016/0198-0149(85)90017-2

Kucera, M., Rosell-Mele, A., Schneider, R., Waelbroeck, C., & Weinelte, M. (2006). Multiproxy Approach for the Reconstruction of the Glacial Ocean surface (MARGO). *Quaternary Science Reviews*, *24*, 813–1107.

Kurahashi-Nakamura, T., Paul, A., & Losch, M. (2017). Dynamical reconstruction of the global ocean state during the Last Glacial Maximum. *Paleoceanography*, *32*, 326–350. https://doi.org/10.1002/2016PA003001

Kwon, E. Y., Hain, M. P., Sigman, D. M., Galbraith, E. D., Sarmiento, J. L., & Toggweiler, J. R. (2012). North Atlantic ventilation of "southern-sourced" deep water in the glacial ocean. *Paleoceanography*, *27*, PA2208. https://doi.org/10.1029/2011PA002211

Labeyrie, L. D., Duplessy, J.-C., Dupratt, J., Juillet-Leclerc, A., Moyes, J., Michel, E., et al. (1992). Changes in the vertical structure of the North Atlantic Ocean between glacial and modern times. *Quaternary Science Reviews*, *11*(4), 401–413. https://doi.org/10.1016/0277-3791(92)90022-Z

Lacerra, M., Lund, D., Yu, J., & Schmittner, A. (2017). Carbon storage in the mid-depth Atlantic during millennial-scale climate events. *Paleoceanography*, *32*, 780–795. https://doi.org/10.1002/2016PA003081

Lear, C. H., Rosenthal, Y., & Slowey, N. (2002). Benthic foraminiferal Mg/Ca-paleothermometry: A revised core-top calibration. *Geochimica et Cosmochimica Acta*, *66*(19), 3375–3387. https://doi.org/10.1016/S0016-7037(02)00941-9

Lewis, E., & Wallace, D. (1998). Program development for CO_2 system calculations carbon dioxide information analysis center, Managed by Lockheed Martin Energy Research Corporation for the US Department of Energy Tennessee.

Lippold, J., Gutjahr, M., Blaser, P., Christner, E., de Carvalho Ferreira, M. L., Mulitza, S., et al. (2016). Deep water provenance and dynamics of the (de) glacial Atlantic meridional overturning circulation. *Earth and Planetary Science Letters*, *445*, 68–78. https://doi.org/10.1016/j.epsl.2016.04.013

Loncke, L., Droz, L., Gaullier, V., Basile, C., Patriat, M., & Roest, W. (2009). Slope instabilities from echo-character mapping along the French Guiana transform margin and Demerara abyssal plain. *Marine and Petroleum Geology*, *26*(5), 711–723. https://doi.org/10.1016/j.marpetgeo.2008.02.010

Lund, D. C., Tessin, A. C., Hoffman, J. L., & Schmittner, A. (2015). Southwest Atlantic water mass evolution during the Last Deglaciation. *Paleoceanography*, *30*, 477–494. https://doi.org/10.1002/2014PA002657

Lynch-Stieglitz, J., Curry, W. B., Oppo, D. W., Ninneman, U. S., Charles, C. D., & Munson, J. (2006). Meridional overturning circulation in the South Atlantic at the Last Glacial Maximum. *Geochemistry, Geophysics, Geosystems*, *7*, Q10N03. https://doi.org/10.1029/2005GC001226

Lynch-Stieglitz, J., Curry, W. B., & Slowey, N. (1999). A geostrophic transport estimate for the Florida Current from the oxygen isotope composition of benthic foraminifera. *Paleoceanography*, *14*, 360–373. https://doi.org/10.1029/1999PA900001

Lynch-Stieglitz, J., Fairbanks, R. G., & Charles, C. D. (1994). Glacial-interglacial history of Antarctic Intermediate Water: Relative strengths of Antarctic versus Indian Ocean sources. *Paleoceanography*, *9*, 7–29. https://doi.org/10.1029/93PA02446

Lynch-Stieglitz, J., Schmidt, M. W., Gene Henry, L., Curry, W. B., Skinner, L. C., Mulitza, S., et al. (2014). Muted change in Atlantic overturning circulation over some glacial-aged Heinrich events. *Nature Geoscience*, *7*(2), 144–150. https://doi.org/10.1038/ngeo2045

Lynch-Stieglitz, J., Stocker, T. F., Broecker, W. S., & Fairbanks, R. G. (1995). The influence of air-sea exchange on the isotopic composition of oceanic carbon: Observations and modeling. *Global Biogeochemical Cycles*, *9*, 653–665. https://doi.org/10.1029/95GB02574

Lynch-Stieglitz, J., , van Geen, A., & Fairbanks, R. G. (1996). Interocean exchange of glacial North Atlantic intermediate water: Evidence from Subantarctic Cd/Ca and carbon isotope measurements. *Paleoceanography*, *11*, 191–201. https://doi.org/10.1029/95pa03772

Makou, M. C., Oppo, D. W., & Curry, W. B. (2010). South Atlantic intermediate water mass geometry for the last glacial maximum from foraminiferal Cd/Ca. *Paleoceanography*, *25*, PA4101. https://doi.org/10.1029/2010PA001962

Marchitto, T. M. (2006). Precise multielemental ratios in small foraminiferal samples determined by sector field ICP-MS. *Geochemistry, Geophysics, Geosystems*, *7*, Q05P13. https://doi.org/10.1029/2005GC001018

Marchitto, T. M., & Broecker, W. S. (2006). Deep water mass geometry in the glacial Atlantic Ocean: A review of constraints from the paleonutrient proxy Cd/Ca. *Geochemistry, Geophysics, Geosystems*, *7*, Q12003. https://doi.org/10.1029/2006GC001323

Marchitto, T. M., Curry, W. B., & Oppo, D. W. (2000). Zinc concentrations in benthic foraminifera reflect seawater chemistry. *Paleoceanography*, *15*, 299–306. https://doi.org/10.1029/1999PA000420

MARGO Project Members (2009). Constraints on the magnitude and patterns of ocean cooling at the Last Glacial Maximum. *Nature Geoscience*, *2*(2), 127–132. https://doi.org/10.1038/ngeo411

Mario, P., & Michel, P. (1998). Origin of late Holocene ne-grained sediments on the French Guiana shelf. *Continental Shelf Research*, *18*(13), 1613–1629. https://doi.org/10.1016/S0278-4343(98)00053-3

Marshall, J., & Speer, K. (2012). Closure of the meridional overturning circulation through Southern Ocean upwelling. *Nature Geoscience*, *5*(3), 171–180. https://doi.org/10.1038/ngeo1391

Marzocchi, A., & Jansen, M. (2017). Connecting Antarctic sea ice to deep ocean circulation in modern and glacial climate simulations. *Geophysical Research Letters*, *44*, 6286–6295. https://doi.org/10.1002/2017GL073936

Matsumoto, K. (2007). Biology-mediated temperature control on atmospheric pCO_2 and ocean biogeochemistry. *Geophysical Research Letters*, *34*, L20605. https://doi.org/10.1029/2007GL031301

McCorkle, D. C., Corliss, B. H., & Farnham, C. A. (1997). Vertical distributions and stable isotopic compositions of live (stained) benthic foraminifera from the North Carolina and California continental margins. *Deep Sea Research Part I: Oceanographic Research Papers*, *44*(6), 983–1024. https://doi.org/10.1016/S0967-0637(97)00004-6

McCorkle, D. C., Martin, P. A., Lea, D. W., & Klinkhammer, G. P. (1995). Evidence of a dissolution effect on benthic foraminiferal shell chemistry: $\delta^{13}C$, Cd/Ca, Ba/Ca, and Sr/Ca results from the Ontong Java Plateau. *Paleoceanography*, *10*, 699–714. https://doi.org/10.1029/95PA01427

McManus, J. F., Francois, R., Gherardi, J.-M., Keigwin, L. D., & Brown-Leger, S. (2004). Collapse and rapid resumption of Atlantic meridional circulation linked to deglacial climate changes. *Nature*, *428*(6985), 834–837. https://doi.org/10.1038/nature02494

Meckler, A. N., Sigman, D. M., Gibson, K. A., François, R., Martínez-García, A., Jaccard, S. L., et al. (2013). Deglacial pulses of deep-ocean silicate into the subtropical North Atlantic Ocean. *Nature*, *495*(7442), 495–498. https://doi.org/10.1038/nature12006

Menviel, L., Yu, J., Joos, F., Mouchet, A., Meissner, K. J., & England, M. H. (2017). Poorly ventilated deep ocean at the Last Glacial Maximum inferred from carbon isotopes: A data-model comparison study. *Paleoceanography*, *32*, 2–17. https://doi.org/10.1002/2016PA003024

Middag, R., van Heuven, S. M. A. C., Bruland, K. W., & de Baar, H. J. W. (2018). The relationship between cadmium and phosphate in the Atlantic Ocean unravelled. *Earth and Planetary Science Letters*, *492*, 79–88. https://doi.org/10.1016/j.epsl.2018.03.046

Milne, A., Landing, W., Bizmis, M., & Morton, P. (2010). Determination of Mn, Fe, CO, Ni, Cu, Zn, Cd and Pb in seawater using high resolution magnetic sector inductively coupled mass spectrometry (HR-ICP-MS). *Analytica Chimica Acta*, *665*(2), 200–207. https://doi.org/10.1016/j.aca.2010.03.027

Muglia, J., & Schmittner, A. (2015). Wind stress increases glacial Atlantic overturning in climate models. *Geophysical Research Letters*, *42*, 9862–9868. https://doi.org/10.1002/2015GL064583

Murray, J. W., & Bowser, S. S. (2000). Mortality, protoplasm decay rate, and reliability of staining techniques to recognize "living" foraminifera: A review. *Journal of Foraminiferal Research*, *30*(1). Retrieved from http://jfr.geoscienceworld.org/content/30/1/), 66–70. https://doi.org/10.2113/0300066

Oppo, D. W., Curry, W. B., & McManus, J. F. (2015). What do benthic $\delta^{13}C$ and $\delta^{18}O$ data tell us about Atlantic circulation during Heinrich Stadial 1? *Paleoceanography*, *30*, 353–368. https://doi.org/10.1002/2014PA002667

Oppo, D. W., & Fairbanks, R. G. (1987). Variability in the deep and intermediate water circulation of the Atlantic Ocean during the past 25,000 years: Northern Hemisphere modulation of the Southern Ocean. *Earth and Planetary Science Letters*, *86*(1), 1–15. https://doi.org/10.1016/0012-821X(87)90183-X

Oppo, D. W., & Fairbanks, R. G. (1989). Carbon isotope composition of tropical surface water during the past 22,000 years. *Paleoceanography*, *4*, 333–351. https://doi.org/10.1029/PA004i004p00333

Oppo, D. W., & Horowitz, M. (2000). Glacial deep water geometry: South Atlantic benthic foraminiferal Cd/Ca and $\delta^{13}C$ evidence. *Paleoceanography*, *15*, 147–160. https://doi.org/10.1029/1999PA000436

Oppo, D. W., & Lehman, S. J. (1993). Mid-depth circulation of the subpolar North Atlantic during the Last Glacial Maximum. *Science*, *259*(5098), 1148–1152. https://doi.org/10.1126/science.259.5098.1148

Ostermann, D. R., & Curry, W. B. (2000). Calibration of stable isotopic data: An enriched $\delta^{18}O$ standard used for source gas mixing detection and correction. *Paleoceanography*, *15*, 353–360. https://doi.org/10.1029/1999PA000411

Pelletier, G., Lewis, E., & Wallace, D. (2005). A calculator for the CO_2 system in seawater for Microsoft Excel/VBA. Washington State Department of Ecology,*Olympia, WA, Brookhaven National Laboratory, Upton, NY*.

Poggemann, D.-W., Hathorne, E. C., Nürnberg, D., Frank, M., Bruhn, I., Reißig, S., et al. (2017). Rapid deglacial injection of nutrients into the tropical Atlantic via Antarctic Intermediate Water. *Earth and Planetary Science Letters*, *463*, 118–126. https://doi.org/10.1016/j.epsl.2017.01.030

Praetorius, S. K., McManus, J. F., Oppo, D. W., & Curry, W. B. (2008). Episodic reductions in bottom-water currents since the last ice age. *Nature Geoscience*, *1*(7), 449–452. https://doi.org/10.1038/ngeo227

Rae, J. W. B., Foster, G. L., Schmidt, D. N., & Elliott, T. (2011). Boron isotopes and B/Ca in benthic foraminifera: Proxies for the deep ocean carbonate system. *Earth and Planetary Science Letters*, *302*(3–4), 403–413. https://doi.org/10.1016/j.epsl.2010.12.034

Reimer, P., Bard, E., Bayliss, A., Beck, J. W., Blackwell, P. G., Ramsey, C. B., et al. (2013). IntCal13 and Marine13 radiocarbon age calibration curves 0–50,000 years cal BP. *Radiocarbon*, *55*(04), 1869–1887. https://doi.org/10.2458/azu_js_rc.55.16947

Rickaby, R. E. M., & Elderfield, H. (2005). Evidence from the high-latitude North Atlantic for variations in Antarctic Intermediate water flow during the last deglaciation. *Geochemistry, Geophysics, Geosystems*, *6*, Q05001. https://doi.org/10.1029/2004GC000858

Rintoul, S. R. (1991). South-Atlantic interbasin exchange. *Journal of Geophysical Research*, *96*, 2675–2692. https://doi.org/10.1029/90jc02422

Robinson, R. S., & Sigman, D. M. (2008). Nitrogen isotopic evidence for a poleward decrease in surface nitrate within the ice age Antarctic. *Quaternary Science Reviews*, *27*(9-10), 1076–1090. https://doi.org/10.1016/j.quascirev.2008.02.005

Rosenthal, Y., Boyle, E. A., Labeyrie, L., & Oppo, D. (1995). Glacial enrichments of authigenic Cd and U in subantarctic sediments: A climatic control on the elements' oceanic budget? *Paleoceanography*, *11*, 191–201. https://doi.org/10.1029/95PA03772

Rosenthal, Y., Field, M. P., & Sherrell, R. M. (1999). Precise determination of element/calcium ratios in calcareous samples using sector field inductively coupled plasma mass spectrometry. *Analytical Chemistry*, *71*(15), 3248–3253. https://doi.org/10.1021/ac981410x

Sarmiento, J. L., Gruber, N., Brzezinski, M. A., & Dunne, J. P. (2004). High-latitude controls of thermocline nutrients and low latitude biological productivity. *Nature*, *427*, 56–60. https://doi.org/10.1038/nature02204.1

Schmidt, G. A. (1999). Forward modeling of carbonate proxy data from planktonic foraminifera using oxygen isotope tracers in a global ocean model. *Paleoceanography*, *14*, 482–497. https://doi.org/10.1029/1999PA900025

Schmittner, A., Bostock, H. C., Cartapanis, O., Curry, W. B., Filipsson, H. L., Galbraith, E. D., et al. (2017). Calibration of the carbon isotope composition ($\delta^{13}C$) of benthic foraminifera. *Paleoceanography*, *32*, 512–530. https://doi.org/10.1002/2016PA003072

Schmittner, A., Gruber, N., Mix, A. C., Key, R. M., Tagliabue, A., & Westberry, T. K. (2013). Biology and air–sea gas exchange controls on the distribution of carbon isotope ratios ($\delta^{13}C$) in the ocean. *Biogeosciences*, *10*(9), 5,793–5,816. https://doi.org/10.5194/BG-10-5793-2013

Schmittner, A., & Lund, D. C. (2015). Early deglacial Atlantic overturning decline and its role in atmospheric CO_2 rise inferred from carbon isotopes ($\delta^{13}C$). *Climate of the Past*, *11*(2), 135–152. https://doi.org/10.5194/cp-11-135-2015

Schmitz, W. J., & McCartney, M. S. (1993). On the North Atlantic circulation. *Reviews of Geophysics*, *31*, 29–49. https://doi.org/10.1029/92RG02583

Shackleton, N. J. (1967). Oxygen isotope analyses and Pleistocene temperatures re-assessed. *Nature*, *215*(5096), 15–17. https://doi.org/10.1038/215015a0

Sherriff-Tadano, S., Abe-Ouchi, A., Yoshimori, M., Oka, A., & Chan, W.-L. (2017). Influence of glacial ice sheets on the Atlantic meridional overturning circulation through surface wind change. *Climate Dynamics*, *50*(7-8), 2881–2903. https://doi.org/10.1007/s00382-017-3780-0

Sigman, D. M., & Boyle, E. A. (2000). Glacial/interglacial variations in atmospheric carbon dioxide. *Nature*, *407*(6806), 859–869. https://doi.org/10.1038/35038000

Sigman, D. M., de Boer, A. M., & Haug, G. H. (2007). Antarctic stratification, atmospheric water vapor, and Heinrich events: A hypothesis for Late Pleistocene deglaciations. *Ocean Circulation: Mechanisms and Impacts*, *173*, 335–349.

Sigman, D. M., Hain, M. P., & Haug, G. H. (2010). The polar ocean and glacial cycles in atmospheric CO_2 concentration. *Nature*, *466*(7302), 47–55. https://doi.org/10.1038/nature09149

Sigman, D. M., & Haug, H. G. (2003). Biological pump in the past, in *Treatise on geochemistry*, 491–528, edited by H. D. Holland & K. K. Turekian (H. Elderfield, volume editor), Elsevier Science, Oxford. https://doi.org/10.1016/B0-08-043751-6/06118-1

Sigman, D. M., Lehman, S. J., & Oppo, D. W. (2003). Evaluating mechanisms of nutrient depletion and ^{13}C enrichment in the intermediate-depth Atlantic during the last ice age. *Paleoceanography*, *18*(3), 1072. https://doi.org/10.1029/2002PA000818

Sikes, E. L., Allen, K. A., & Lund, D. C. (2017). Enhanced $\delta^{13}C$ and $\delta^{18}O$ differences between the South Atlantic and South Pacific during the last glaciation: The deep gateway hypothesis. *Paleoceanography*, *32*, 1,000–1,017. https://doi.org/10.1002/2017PA003118

Skinner, L. C., Primeau, F., Freeman, E., de la Fuente, M., Goodwin, P. A., Gottschalk, J., et al. (2017). Radiocarbon constraints on the glacial ocean circulation and its impact on atmospheric CO_2. *Nature Communications*, *8*(May), 16,010. https://doi.org/10.1038/ncomms16010

Slowey, N. C., & Curry, W. B. (1992). Enhanced ventilation of the North Atlantic subtropical gyre themocline during the last glaciation. *Nature*, *358*(6388), 665–668. https://doi.org/10.1038/358665a0

Spero, H. J., & Williams, D. F. (1988). Extracting environmental information from planktonic foraminiferal $\delta^{13}C$ data. *Nature*, *335*(6192), 717–719. https://doi.org/10.1038/335717a0

Spooner, P. T., Thornalley, D. J. R., & Ellis, P. (2018). Grain size constraints on glacial circulation in the Southwest Atlantic. *Paleoceanography and Paleoclimatology*, *33*, 21–30. https://doi.org/10.1002/2017PA003232

Talley, L. D. (1999). Some aspects of ocean heat transport by the shallow, intermediate and deep overturning circulations. In P. U. Clark, R. S. Webb, & L. D. Keigwin (Eds.), *Mechanisms of global climate change at millennial time scales* (pp. 1–22). Washington, DC: American Geophysical Union.

Tessin, A. C., & Lund, D. C. (2013). Isotopically depleted carbon in the mid-depth South Atlantic during the last deglaciation. *Paleoceanography*, *28*, 296–306. https://doi.org/10.1002/palo.20026

Thornalley, D. J. R., Elderfield, H., & McCave, I. N. (2010). Intermediate and deep water paleoceanography of the northern North Atlantic over the past 21,000 years. *Paleoceanography*, *25*, PA1211. https://doi.org/10.1029/2009PA001833

Toggweiler, J. R. (1999). Variation of atmospheric CO_2 by ventilation of the ocean's deepest water. *Paleoceanography*, *14*, 571–588. https://doi.org/10.1029/1999PA900033

Tuerena, R. E., Ganeshram, R. S., Geibert, W., Fallick, A. E., Dougans, J., Tait, A., et al. (2015). *Global Biogeochemical Cycles*, *29*, 1830–1844. https://doi.org/10.1002/2015GB005164.Received

Voigt, I., Cruz, A. P. S., Mulitza, S., Chiessi, C. M., Mackensen, A., Lippold, J., et al. (2017). Variability in mid-depth ventilation of the western Atlantic Ocean during the last deglaciation. *Paleoceanography*, *32*, 948–965. https://doi.org/10.1002/2017PA003095

Weldeab, S., Friedrich, T., Timmermann, A., & Schneider, R. R. (2016). Strong middepth warming and weak radiocarbon imprints in the equatorial Atlantic during Heinrich 1 and Younger Dryas. *Paleoceanography*, *31*, 1070–1082. https://doi.org/10.1002/2016PA002957

Xie, R. C., Galer, S. J. G., Abouchami, W., Rijkenberg, M. J. A., De Jong, J., de Baar, H. J. W., et al. (2015). The cadmium–phosphate relationship in the western South Atlantic—The importance of mode and intermediate waters on the global systematics. *Marine Chemistry*, *177*, 110–123. https://doi.org/10.1016/j.marchem.2015.06.011

Xie, R. C., Marcantonio, F., & Schmidt, M. W. (2014). Reconstruction of intermediate water circulation in the tropical North Atlantic during the past 22,000 years. *Geochimica et Cosmochimica Acta*, *140*, 455–467. https://doi.org/10.1016/j.gca.2014.05.041

Yu, J., Broecker, W. S., Elderfield, H., Jin, Z., McManus, J., & Zhang, F. (2010). Loss of carbon from the deep sea since the Last Glacial Maximum. *Science*, *330*(6007), 1084–1087. https://doi.org/10.1126/science.1193221

Yu, J., & Elderfield, H. (2007). Benthic foraminiferal B/Ca ratios reflect deep water carbonate saturation state. *Earth and Planetary Science Letters*, *258*(1–2), 73–86. https://doi.org/10.1016/j.epsl.2007.03.025

Yu, J., Elderfield, H., & Piotrowski, A. M. (2008). Seawater carbonate ion- $\delta^{13}C$ systematics and application to glacial-interglacial North Atlantic Ocean circulation. *Earth and Planetary Science Letters*, *271*(1–4), 209–220. https://doi.org/10.1016/j.epsl.2008.04.010